High order absolutely convergent fast sweeping methods with multi-resolution WENO local solvers for Eikonal and factored Eikonal equations

Rentian Hu[1], Yong-Tao Zhang[2]

Abstract

Fast sweeping methods are a class of efficient iterative methods developed in the literature to solve steady-state solutions of hyperbolic partial differential equations (PDEs). In (Zhang et al. 2006 [35]; Xiong et al. 2010 [31]), high order accuracy fast sweeping schemes based on classical weighted essentially non-oscillatory (WENO) local solvers were developed for solving static Hamilton-Jacobi equations. However, since high order classical WENO methods (e.g., fifth order and above) often suffer from difficulties in their convergence to steady-state solutions, iteration residues of high order fast sweeping schemes with these local solvers may hang at a level far above round-off errors even after many iterations. This issue makes it difficult to determine the convergence criterion for the high order fast sweeping methods and challenging to apply the methods to complex problems. Motivated by the recent work on absolutely convergent fast sweeping method for steady-state solutions of hyperbolic conservation laws in (Li et al. 2021 [11]), in this paper we develop high order fast sweeping methods with multi-resolution WENO local solvers for solving Eikonal equations, an important class of static Hamilton-Jacobi equations. Based on such kind of multi-resolution WENO local solvers with unequal-sized sub-stencils, iteration residues of the designed high order fast sweeping methods can settle down to round-off errors and achieve the absolute convergence. In order to obtain high order accuracy for problems with singular source-point, we apply the factored Eikonal approach developed in the literature and solve the resulting factored Eikonal equations by the new high order WENO fast sweeping methods. Extensive numerical experiments are performed to show the accuracy, computational efficiency, and advantages of the new high order fast sweeping schemes for solving static Hamilton-Jacobi equations.

Key Words: High order accuracy fast sweeping methods, Weighted essentially non-oscillatory (WENO) schemes, Multi-resolution WENO schemes, Static Hamilton-Jacobi equations, Factored Eikonal equations

[1]Department of Applied and Computational Mathematics and Statistics, University of Notre Dame, Notre Dame, IN 46556, USA. E-mail: rhu@nd.edu

[2]Corresponding author. Department of Applied and Computational Mathematics and Statistics, University of Notre Dame, Notre Dame, IN 46556, USA. E-mail: yzhang10@nd.edu

1 Introduction

In this paper, we develop new high order accuracy finite difference fast sweeping methods for solving static Hamilton-Jacobi (H-J) equations [2], especially Eikonal equations. The two-dimensional (2D) static H-J equations have the following general form

$$\begin{cases} H(\phi_x, \phi_y) = f(x,y), & (x,y) \in \Omega \setminus \Gamma, \\ \phi(x,y) = g(x,y), & (x,y) \in \Gamma \subset \Omega, \end{cases} \tag{1}$$

where $\phi(x,y)$ is the unknown function, and $f(x,y)$, $g(x,y)$ are given functions. H is the Hamiltonian, Ω is a computational domain in R^2, and Γ is a subset of Ω. Boundary conditions are defined on Γ. Note that although we focus on 2D problems in this paper, extension of the methods to solve higher dimensional problems is straightforward, due to the dimension-by-dimension property of finite difference methods. Among the static H-J equations, a very important class of them are the Eikonal equations. For example, the standard isotropic Eikonal equations have the form

$$\begin{cases} |\nabla \phi(x,y)| = f(x,y), & (x,y) \in \Omega \setminus \Gamma, \\ \phi(x,y) = g(x,y), & (x,y) \in \Gamma \subset \Omega, \end{cases} \tag{2}$$

where $f(x,y)$ is a positive function. The numerical computations of static H-J equations, especially the Eikonal equations appear in many applications, such as optimal control, image processing and computer vision, geometric optics, seismic waves, level set methods, etc.

Due to nonlinearity of the PDEs and possible singularities in their solutions, it is challenging to design efficient and high order accurate numerical methods for solving static H-J equations such as the Eikonal equations (2). In the literature, a popular approach is to first discretize the PDE (2) into a nonlinear system by an appropriate scheme, and then design a fast numerical method to solve the nonlinear system. Among such methods are the fast marching method and the fast sweeping method. The fast marching method uses the Dijkstra's algorithm [3] and updates the solution by following the Eikonal equations' causality sequentially, e.g., see [23, 24, 25]. In the fast sweeping method [37, 36, 8, 19, 20, 4], Gauss-Seidel iterations with alternating orderings are combined with upwind schemes. Different from the fast marching method, the fast sweeping method is an iterative method and follows the Eikonal equations' causality along characteristics in a parallel way, i.e., each Gauss-Seidel iteration with a specific sweeping ordering covers a family of characteristics in a certain direction simultaneously. The iterative framework of fast sweeping method provides good flexibility to incorporate high order accuracy schemes for hyperbolic PDEs, such as weighted essentially non-oscillatory (WENO) methods [35, 31] or discontinuous Galerkin (DG) methods [9, 32, 29], into it for developing high order fast sweeping methods. As a generalization of the high order fast sweeping methods [35], fixed-point fast sweeping methods were designed to solve static H-J equations in [34]. They were applied to sparse-grid WENO schemes for efficiently solving multidimensional Eikonal equations in [17], and in [30, 11], high order accuracy WENO fixed-point fast sweeping methods for efficiently solving steady-state problems of compressible flows modeled by

nonlinear hyperbolic conservation laws were developed. Recently, a second-order distributed memory parallel fast sweeping method was developed to solve large problems modeled by Eikonal equations in [27]. In [5], hybrid fast sweeping methods for solving anisotropic Eikonal equation in two-dimensional tilted transversely isotropic media were designed. To solve the generalized Eikonal equation arising from wave propagation in an isotropic acoustic medium occupied by a moving fluid, a Newton-type Gauss-Seidel Lax-Friedrichs fast sweeping method was proposed and studied in [12].

High order WENO fast sweeping methods [35, 34, 31] have a nice property that they are explicit, which is achieved by a strategy designed in the iterative schemes to avoid directly solving very complicated local nonlinear equations derived from high order WENO discretizations. Hence they can be easily adopted to solve complex hyperbolic systems stably with a high order accuracy. There are two important issues to be resolved when high order WENO fast sweeping methods are designed. One is that high order classical WENO methods (e.g., fifth order and above) often suffer from difficulties in their convergence to steady-state solutions, which make the iteration residues of high order fast sweeping schemes based on such WENO local solvers [31] hang at a level far above round-off errors even after many iterations. This issue makes it difficult to determine the convergence criterion for the high order WENO fast sweeping methods and challenging to apply the methods to complex problems. Recently, studies on high order WENO schemes with unequal-sized sub-stencils reveal that they improve the convergence of high order WENO schemes with equal-sized sub-stencils to steady-state solutions [38, 21]. In [39], a new type of WENO schemes, called multi-resolution WENO (MR-WENO) schemes, were developed to solve hyperbolic conservation laws. This class of WENO schemes are also based on unequal-sized sub-stencils. Specifically, the MR-WENO schemes use the information defined on a hierarchy of nested central spatial stencils to construct polynomials for sustaining high order approximations at the boundary points of a computational cell, which makes the degrading of accuracy near discontinuities of the solution be gradual and improves the resolution of numerical solution. The MR-WENO schemes exhibit interesting properties such as their simplicity in constructing linear weights, which in general can be taken as arbitrary positive numbers with the only requirement that their sum equals 1. They were applied to solve time-dependent Hamilton-Jacobi equations on moving meshes in [13]. In [11], the MR-WENO schemes were incorporated in fixed-point fast sweeping methods for solving steady-state problems of hyperbolic conservation laws, and it was found that the residue of fast sweeping iterations can be driven to machine zero / round-off errors. The property of an iterative scheme that the residue of its iterations can settle down to machine zero or round-off error level in a finite number of iterations is called "absolute convergence" in [11]. Motivated by this work, in this paper we develop high order fast sweeping methods with MR-WENO local solvers for solving static Hamilton-Jacobi equations and verify that the absolute convergence can be maintained. The second issue is to deal with numerical boundary conditions near inflow boundaries in high order WENO fast sweeping methods, since high order WENO discretization involves a wider stencil than a low order scheme. For problems in which the inflow boundary Γ is a smooth curve or the solution does not have singularity near Γ, the Richardson extrapolation procedure or the inverse Lax-Wendroff procedure as in [6, 31, 10] provide accurate numerical boundary conditions. However, for problems

with a singular source-point inflow boundary, the factored Eikonal approach developed in [4, 14] is more effective to treat the inflow boundary and achieve high order accuracy. The factored Eikonal approach decomposes the solution of original Eikonal equation to a non-smooth part and a smooth part. The non-smooth part of solution carries the upwind source singularity which causes the pollution to the accuracy of numerical solution, and it can be derived analytically (e.g., the distance function to the source-point). The original Eikonal equation is then transformed to a factored Eikonal equation for the smooth part of the solution, which does not have the upwind source singularity any more. Hence, high order fast sweeping methods can be applied to the factored Eikonal equation to obtain desired accuracy. In this paper, we apply the developed high order MR-WENO fast sweeping methods to solve factored Eikonal equations for these problems with a singular source-point inflow boundary, and maintain the high order accuracy of numerical solution of the original Eikonal equation.

The organization of the paper is as follows. The detailed description of the new absolutely convergent MR-WENO fast sweeping methods for static H-J equations and the approaches to treat inflow boundaries is provided in Section 2. In Section 3, we perform numerical experiments to study the proposed methods, and carry out comparisons of different methods. Extensive numerical examples, including isotropic and anisotropic Eikonal equations, and the corresponding factored Eikonal equations for problems with singular source-point, are solved to show the accuracy, computational efficiency, and absolute convergence of the presented high order MR-WENO fast sweeping schemes. Concluding remarks are given in Section 4.

2 Description of the numerical methods

In this section, we describe the development of the new high order WENO fast sweeping methods for solving the static Hamilton-Jacobi equations, based on the framework of high order fast sweeping methods in [35, 31] and the multi-resolution WENO methods in [39].

2.1 The local solvers

The computational domain Ω is partitioned by a Cartesian grid $\{(x_i, y_j), 1 \leq i \leq N, 1 \leq j \leq M\}$, with uniform grid sizes h_x and h_y in the x and y directions respectively. For simplicity of the description, we take $h_x = h_y = h$. The Hamiltonian H in the equation (1) is discretized by a monotone numerical Hamiltonian $\hat{H}$ [18] for finding viscosity numerical solution. As in [35], two types of numerical Hamiltonian are used in this paper: the Godunov numerical Hamiltonian and the Lax-Friedrichs numerical Hamiltonian. For the Eikonal equations (2), the Godunov numerical Hamiltonian is easily applied and explicit form of solutions of local solvers can be derived, which results in efficient schemes [36, 35]. For a general static H-J equation (1), it is more suitable to use the Lax-Friedrichs numerical Hamiltonian to form a fast sweeping method [8, 35], which is adopted to solve the factored Eikonal equations in the following sections.

For the Eikonal equation (2) with the Godunov numerical Hamiltonian discretization, the local solver using a high order approximation to update the new solution at

the grid point (x_i, y_j) is derived in [35] and has the following form:

$$\phi_{i,j}^{new} = \begin{cases} \min(\phi_{i,j}^{x\ \min}, \phi_{i,j}^{y\ \min}) + f_{i,j}h, & |\phi_{i,j}^{x\ \min} - \phi_{i,j}^{y\ \min}| \geq f_{i,j}h, \\ \dfrac{\phi_{i,j}^{x\ \min} + \phi_{i,j}^{y\ \min} + (2f_{i,j}^2h^2 - (\phi_{i,j}^{x\ \min} - \phi_{i,j}^{y\ \min})^2)^{0.5}}{2}, & \text{otherwise}, \end{cases} \tag{3}$$

where $\phi_{i,j}^{new}$ denotes the to-be-updated numerical solution for ϕ at the grid point (x_i, y_j), $f_{i,j} = f(x_i, y_j)$, and

$$\begin{cases} \phi_{i,j}^{x\ \min} = \min(\phi_{i,j}^{old} - h \cdot (\phi_x)_{i,j}^-, \phi_{i,j}^{old} + h \cdot (\phi_x)_{i,j}^+), \\ \phi_{i,j}^{y\ \min} = \min(\phi_{i,j}^{old} - h \cdot (\phi_y)_{i,j}^-, \phi_{i,j}^{old} + h \cdot (\phi_y)_{i,j}^+). \end{cases} \tag{4}$$

Here $\phi_{i,j}^{old}$ denotes the currently available value for ϕ at the same grid point (x_i, y_j). $(\phi_x)_{i,j}^-$, $(\phi_x)_{i,j}^+$, $(\phi_y)_{i,j}^-$ and $(\phi_y)_{i,j}^+$ are high order approximations for the one-sided derivatives of ϕ at (x_i, y_j). In this paper, they are computed by the high order multi-resolution WENO schemes described in the following. Note that according to the philosophy of Gauss-Seidel iterations in the fast sweeping methods, we always use the newest available values of ϕ in the multi-resolution WENO schemes' stencils to compute these approximations of derivatives. Namely, a numerical value (e.g. $\phi_{k,l}$) used in the multi-resolution WENO schemes' stencils could be the value of the previous iteration step, or the new value which has been updated and available in the current iteration step, depending on the current sweeping direction of the iteration.

For the general static H-J equations (1), the Lax-Friedrichs numerical Hamiltonian is used, which has the form

$$\hat{H}^{LF}(u^-, u^+; v^-, v^+) = H\left(\frac{u^- + u^+}{2}, \frac{v^- + v^+}{2}\right) - \frac{1}{2}\alpha_x(u^+ - u^-) - \frac{1}{2}\alpha_y(v^+ - v^-)$$

with

$$\alpha_x = \max_{\substack{A \leq u \leq B \\ C \leq v \leq D}} |H_1(u, v)|, \quad \alpha_y = \max_{\substack{A \leq u \leq B \\ C \leq v \leq D}} |H_2(u, v)|. \tag{5}$$

Here u and v correspond to ϕ_x and ϕ_y respectively. $H_i(u, v)$ is the partial derivative of H with respect to the ith argument, or the Lipschitz constant of H with respect to the ith argument. $[A, B]$ is the value range for $u^{\pm}$, and $[C, D]$ is the value range for $v^{\pm}$. The local solver using the Lax-Friedrichs numerical Hamiltonian and a high order approximation to update the new solution at the grid point (x_i, y_j) is derived in [35] and has the following form:

$$\begin{aligned} \phi_{i,j}^{new} = \left(\frac{h}{\alpha_x + \alpha_y}\right) \Bigg[f - H\left(\frac{(\phi_x)_{i,j}^- + (\phi_x)_{i,j}^+}{2}, \frac{(\phi_y)_{i,j}^- + (\phi_y)_{i,j}^+}{2}\right) \\ + \alpha_x \frac{(\phi_x)_{i,j}^+ - (\phi_x)_{i,j}^-}{2} + \alpha_y \frac{(\phi_y)_{i,j}^+ - (\phi_y)_{i,j}^-}{2} \Bigg] + \phi_{i,j}^{old}. \end{aligned} \tag{6}$$

Again $(\phi_x)_{i,j}^-$, $(\phi_x)_{i,j}^+$, $(\phi_y)_{i,j}^-$ and $(\phi_y)_{i,j}^+$ are high order approximations for the one-sided derivatives of ϕ at (x_i, y_j), and they are computed by the high order multi-resolution WENO schemes in this paper, with the philosophy of Gauss-Seidel iterations applied.

Now we describe the procedure of computing high order approximations of the one-sided derivatives $(\phi_x)^-_{i,j}$ $(\phi_x)^+_{i,j}$, $(\phi_y)^-_{i,j}$ and $(\phi_y)^+_{i,j}$ in Eq. (4) and Eq. (6). Specifically, the third order multi-resolution WENO (MR-WENO3) scheme and the fifth order multi-resolution WENO (MR-WENO5) scheme are used. We present the construction of WENO approximations on the cell $I_c = [x_i, x_{i+1}]$, with the computational stencil of the MR-WENO3 scheme shown in Fig. 1 and the computational stencil of the MR-WENO5 scheme shown in Fig. 2. They are used to compute $(\phi_x)^+_{i,j}$ and $(\phi_x)^-_{i+1,j}$ then. Note that due to the nice dimension-by-dimension property of finite difference methods, we only need to simply describe the methods for the one-dimensional case. So in the following description, we omit the notations for the y-direction and just denote the grid points by their indexes (e.g., the grid point i means x_i, etc.)

- Step 1: The hierarchical central spatial stencils $T_1 = \{i, i+1\}$ and $T_2 = \{i-1, i, i+1, i+2\}$ are chosen for the MR-WENO3 scheme (see Fig. 1). For the MR-WENO5 scheme, one more stencil $T_3 = \{i-2, i-1, i, i+1, i+2, i+3\}$ is needed (see Fig. 2). We interpolate the point values of ϕ on these nodes of stencils to obtain a first degree polynomial $p_1(x)$ on T_1, a third degree polynomial $q_2(x)$ on T_2, and a fifth degree polynomial $q_3(x)$ on T_3.

- Step 2: Define another third degree polynomial by $p_2(x) = \dfrac{1}{\gamma_{2,2}} q_2(x) - \dfrac{\gamma_{1,2}}{\gamma_{2,2}} p_1(x)$.
  For the MR-WENO5 scheme, we also define another fifth degree polynomial by $p_3(x) = \dfrac{1}{\gamma_{3,3}} q_3(x) - \dfrac{\gamma_{1,3}}{\gamma_{3,3}} p_1(x) - \dfrac{\gamma_{2,3}}{\gamma_{3,3}} p_2(x)$.
  Here $\gamma_{1,2}$ and $\gamma_{2,2}$ are the linear weights, which can be chosen as any positive numbers with the only condition that their sum equals 1. Similarly, the linear weights $\gamma_{1,3}, \gamma_{2,3}$, and $\gamma_{3,3}$ are chosen such that their sum is 1. Following the practice in [39] for a good balance of accuracy in smooth regions and oscillation control near singularities, we choose
  $\gamma_{1,2} = \dfrac{1}{11}, \gamma_{2,2} = \dfrac{10}{11}$, and
  $\gamma_{1,3} = \dfrac{1}{111}, \gamma_{2,3} = \dfrac{10}{111}, \gamma_{3,3} = \dfrac{100}{111}$.

- Step 3: Compute the smoothness indicators β_1, β_2 and β_3 to measure how smooth the derivatives of $p_1(x), p_2(x)$, and $p_3(x)$ are in the cell I_c respectively. The similar definition as in [7] is used, except that we start the measurement of smoothness from the second derivative rather than the first derivative, following the approach for solving H-J equations (e.g. [33]). The smoothness indicators β_2 and β_3 are given by
$$\beta_k = \sum_{\alpha=2}^{2k-1} \int_{x_i}^{x_{i+1}} h^{2\alpha-1} \left(\frac{d^\alpha p_k(x)}{dx^\alpha} \right)^2 dx, \qquad k = 2, 3. \tag{7}$$
  For the first degree polynomial $p_1(x)$, if the formula (7) is used directly, $\beta_1 = 0$ is obtained. As that pointed out in [39], usage of $\beta_1 = 0$ does not cause any problems in schemes' accuracy, but may lead to more smeared shock transitions. So similar to the approach in [39, 13], the size of β_1 is increased slightly. This is done by first adding either the left neighboring node $i-1$ or the right neighboring

node $i+2$ into the stencil T_1 to get two quadratic interpolation polynomials, and using the formula (7) to calculate their smoothness indicators

$$\beta(1) = (\phi_{i+1,j} - 2\phi_{i,j} + \phi_{i-1,j})^2,$$
$$\beta(2) = (\phi_{i+2,j} - 2\phi_{i+1,j} + \phi_{i,j})^2.$$

Since it is preferred to increase β_1 from zero as little as possible, we choose the smaller one of them as the final value of β_1:

$$\beta_1 = \min(\beta(1), \beta(2)). \tag{8}$$

- Step 4: Compute the nonlinear weights following the WENO-JS strategy [7] for the MR-WENO3 scheme as

$$w_k^{(3)} = \frac{\tilde{w}_k^{(3)}}{\sum_{l=1}^{2} \tilde{w}_l^{(3)}}, \quad k = 1, 2, \tag{9}$$

where

$$\tilde{w}_l^{(3)} = \frac{\gamma_{l,2}}{(\epsilon + \beta_l)^2}, \quad l = 1, 2, \tag{10}$$

and for the MR-WENO5 scheme as

$$w_k^{(5)} = \frac{\tilde{w}_k^{(5)}}{\sum_{l=1}^{3} \tilde{w}_l^{(5)}}, \quad k = 1, 2, 3, \tag{11}$$

where

$$\tilde{w}_l^{(5)} = \frac{\gamma_{l,3}}{(\epsilon + \beta_l)^2}, \quad l = 1, 2, 3. \tag{12}$$

Here ϵ is a small number, and in our simulations it is chosen to be $\epsilon = 10^{-3}$ unless otherwise indicated in specific examples.

- Step 5: The final MR-WENO3 approximations are

$$(\phi_x)_{i,j}^{+} = \sum_{k=1}^{2} w_k^{(3)} \frac{dp_k}{dx}(x_i), \tag{13}$$

$$(\phi_x)_{i+1,j}^{-} = \sum_{k=1}^{2} w_k^{(3)} \frac{dp_k}{dx}(x_{i+1}), \tag{14}$$

and the MR-WENO5 approximations are

$$(\phi_x)_{i,j}^{+} = \sum_{k=1}^{3} w_k^{(5)} \frac{dp_k}{dx}(x_i), \tag{15}$$

$$(\phi_x)_{i+1,j}^{-} = \sum_{k=1}^{3} w_k^{(5)} \frac{dp_k}{dx}(x_{i+1}). \tag{16}$$

The computations of $(\phi_y)^+_{i,j}$ and $(\phi_y)^-_{i,j+1}$ are analogous.

Remark 1. Note that different from [39, 13] in which the computations of nonlinear weights adopt the WENO-Z strategy [1], here the classical WENO-JS strategy [7] is used in the step 4 when computing nonlinear weights. The motivation of doing this is that we aim to use a uniform set of parameters in the WENO approximations (e.g. linear weights, ϵ and the power parameter in nonlinear weights) for the same class of problems (e.g. the isotropic Eikonal equations), with the goal to have problem-independent parameters in the local solvers. Via numerical experiments, we find that if the WENO-JS strategy is used, a uniform set of parameters in the MR-WENO5 approximation can be taken to achieve the desired accuracy and convergence of the fast sweeping methods, for all examples of the isotropic Eikonal equations in this paper. However, if the WENO-Z nonlinear weights are used in the step 4, the parameters in nonlinear weights have to be adjusted in different problems to obtain satisfactory accuracy and convergence results for the proposed fast sweeping methods. Since the WENO-Z schemes improve the accuracy of the classical WENO-JS schemes at smooth extrema or critical points, it will be an interesting topic for our future work to explore more about this and find an approach to design the proposed methods using the WENO-Z nonlinear weights with problem-independent parameters.

2.2 Inflow boundary treatments

In this section, we describe methods adopted in this paper to treat inflow boundary. If a grid point is at the inflow boundary Γ, the numerical solution $\phi_{i,j}$ at the point is prescribed by the physical boundary condition and fixed during the fast sweeping iterations. However, for some points near inflow boundary Γ (i.e., the points whose distances to Γ is less than or equal to $2h$ for the MR-WENO3 scheme, or the points whose distances to Γ is less than or equal to $3h$ for the MR-WENO5 scheme), due to wide stencil of a WENO scheme, these points usually need to be considered as part of the inflow boundary and accurate approximations for values on them need to be provided. As pointed out in [35], this is for the maintenance of the desired accuracy of the fast sweeping schemes. Following [31], we use the Richardson extrapolation procedure or the inverse Lax-Wendroff procedure to obtain a third order or a fifth order accuracy approximation for most of the cases that Γ is a smooth curve or the solution does not have singularity near Γ. On the other hand, for the problems with a singular source-point inflow boundary, we use a different approach from [35, 31], the factored Eikonal approach in [4, 14], to treat the inflow boundary and achieve high order accuracy. In the following we describe these approaches in details.

2.2.1 Richardson extrapolation procedure

The Richardson extrapolation procedure is to first obtain several solutions using the first order fast sweeping iterations with different mesh sizes, then the Richardson extrapolation is used to obtain high order accurate numerical values for those grid points near the inflow boundary Γ. For such a point e.g. (x, y), assume that I is the exact solution at (x, y) and I_h is the numerical solution of the first order fast sweeping scheme

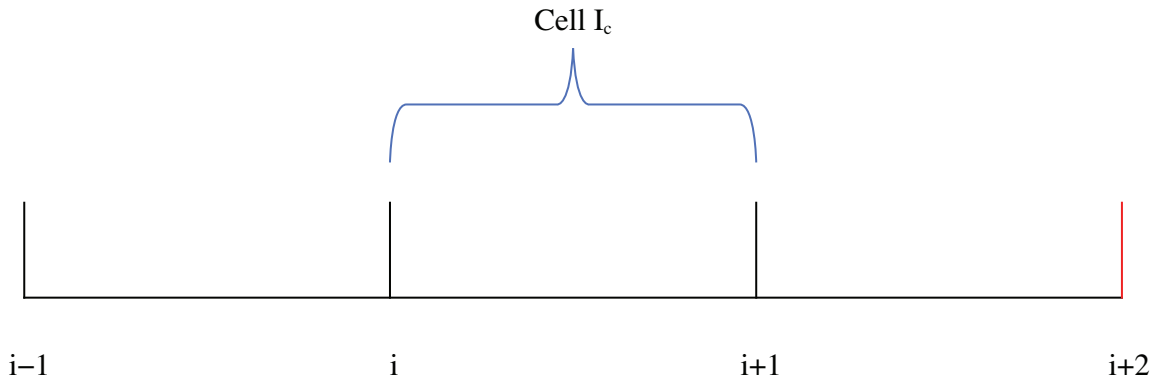

Figure 1: The stencil of the MR-WENO3 scheme for approximations on the cell I_c.

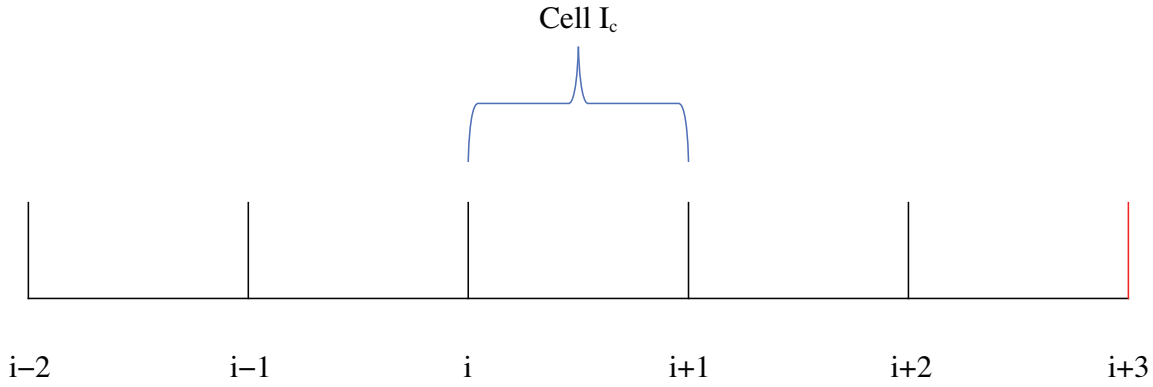

Figure 2: The stencil of the MR-WENO5 scheme for approximations on the cell I_c.

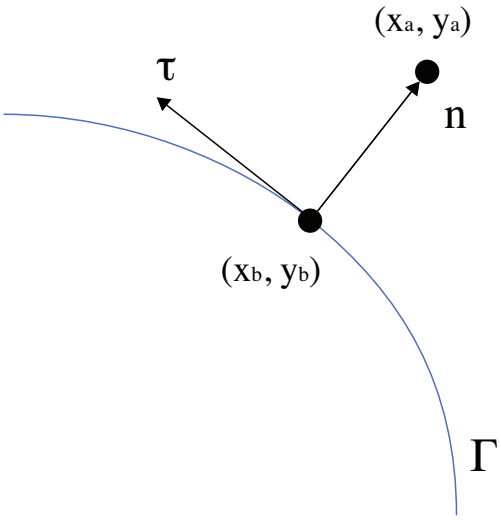

Figure 3: Inverse Lax-Wendroff procedure for an inflow boundary Γ.

[36] with mesh size h. We calculate five first order numerical approximations at the location (x, y) with mesh sizes $h, h/2, h/4, h/8, h/16$: $I_h, I_{h/2}, I_{h/4}, I_{h/8}, I_{h/16}$. When the exact solution is smooth enough at (x, y), the Richardson extrapolation [31] gives a fifth order approximation to I as the following

$$\tilde{I}_h = \frac{1}{315} I_h - \frac{2}{21} I_{h/2} + \frac{8}{9} I_{h/4} - \frac{64}{21} I_{h/8} + \frac{1024}{315} I_{h/16}. \tag{17}$$

The fifth order approximation (17) is used for the local solver with the MR-WENO5 scheme. Similarly, the third order Richardson extrapolation [6] approximation to I is

$$\tilde{I}_h = \frac{1}{3} I_h - 2 I_{h/2} + \frac{8}{3} I_{h/4}, \tag{18}$$

which is used for the local solver with the MR-WENO3 scheme. This boundary treatment method is suitable for a case that the inflow boundary is a single point and the solution is smooth around the source point. Since the solution is smooth in the neighborhood of the source point, the Richardson extrapolations (17) and (18) give stable high order accuracy approximations of numerical values for those grid points near the source point.

2.2.2 Inverse Lax-Wendroff procedure

The inverse Lax-Wendroff procedure for inflow boundary treatment of the H-J equations in [6, 31] is to repeatedly use the PDE, the physical boundary condition and the Taylor expansion, to obtain high order approximations of numerical values for those grid points near the inflow boundary Γ. Here we illustrate the details of the procedure. Considering the inflow boundary Γ as in Fig. 3, we denote the parametric equations of

Γ by $x = x(s), y = y(s)$ with a parameter s, and the inflow boundary condition on Γ is given by

$$\phi(x(s), y(s)) = g(x(s), y(s)). \tag{19}$$

For example, (x_a, y_a) is the point for which we are looking for a high order approximation of numerical value. We first identify the point (x_b, y_b) on the boundary Γ such that the outward normal at (x_b, y_b) goes through (x_a, y_a). See Fig. 3 for an illustration. The coordinates of the point (x_b, y_b) and the outward normal are obtained from the given geometry of Γ. A local coordinate system (n, τ) at the point (x_b, y_b) is set up as

$$\begin{pmatrix} n \\ \tau \end{pmatrix} = \begin{pmatrix} \cos\theta & \sin\theta \\ -\sin\theta & \cos\theta \end{pmatrix} \begin{pmatrix} x \\ y \end{pmatrix}$$

where θ is the angle between the outward normal vector and the x-axis. The n-axis has the same direction as the outward normal and the τ-axis is the tangential direction. Under this local coordinate system, the function $\phi(x, y)$ is transformed to $\hat{\phi}(n, \tau)$. Denote the coordinates of (x_b, y_b) under the local coordinate system by (n_b, τ_b), and the coordinates of (x_a, y_a) under the local coordinate system by (n_a, τ_a). The fifth order Taylor expansion to the numerical value of ϕ at the grid point (x_a, y_a) gives

$$\begin{aligned} \phi(x_a, y_a) = \hat{\phi}(n_b, \tau_b) + (n_a - n_b)\hat{\phi}_n(n_b, \tau_b) + \frac{(n_a - n_b)^2}{2!}\hat{\phi}_{nn}(n_b, \tau_b) \\ + \frac{(n_a - n_b)^3}{3!}\hat{\phi}_{nnn}(n_b, \tau_b) + \frac{(n_a - n_b)^4}{4!}\hat{\phi}_{nnnn}(n_b, \tau_b) + O((n_a - n_b)^5), \end{aligned} \tag{20}$$

where $\hat{\phi}_n(n_b, \tau_b)$ is the first order derivative in the normal direction (i.e., the n-axis) at the point (n_b, τ_b) (i.e., (x_b, y_b)), and similarly for the second, the third, and the fourth order derivatives in the normal direction.

Here, the first term at the right hand side is directly obtained by the given inflow boundary condition (19), namely $\hat{\phi}(n_b, \tau_b) = \phi(x_b, y_b) = g(x_b, y_b)$. The remaining normal derivative terms are found by using the PDE and the condition (19) together. For $\hat{\phi}_n(n_b, \tau_b)$, we use the PDE (1) under the local coordinate system, evaluated at the point (n_b, τ_b):

$$\widetilde{H}(\hat{\phi}_n(n_b, \tau_b), \hat{\phi}_\tau(n_b, \tau_b)) = \hat{f}(n_b, \tau_b). \tag{21}$$

The tangential derivative value $\hat{\phi}_\tau(n_b, \tau_b)$ can be found explicitly using the inflow boundary condition (19) and the parametric equations of Γ. Then we proceed to solve for $\hat{\phi}_n(n_b, \tau_b)$ using the equation (21). Since the equation is usually nonlinear (e.g., it is a quadratic equation for an Eikonal equation), there might be more than one solution. As suggested in [6, 31], in this case we choose the solution so that

$$\partial_u \widetilde{H}(\hat{\phi}_n(n_b, \tau_b), \hat{\phi}_\tau(n_b, \tau_b)) > 0, \tag{22}$$

where ∂_u refers to the partial derivative with respect to the first argument in $\widetilde{H}(u, v)$. This is consistent with the condition that the boundary Γ is an inflow boundary. If we still cannot pin down a solution, then the solution which is closest to the value from the first order fast sweeping solution [8, 36] at the same grid point is chosen.

To find the second order normal derivative value $\hat{\phi}_{nn}(n_b, \tau_b)$, we first differentiate the PDE (1) with respect to τ under the local coordinate system (see the equation (21)), and then evaluate it at (n_b, τ_b), which gives

$$\partial_u \widetilde{H}(\hat{\phi}_n(n_b,\tau_b), \hat{\phi}_\tau(n_b,\tau_b))\hat{\phi}_{n\tau}(n_b,\tau_b) + \partial_v \widetilde{H}(\hat{\phi}_n(n_b,\tau_b), \hat{\phi}_\tau(n_b,\tau_b))\hat{\phi}_{\tau\tau}(n_b,\tau_b) = \hat{f}_\tau(n_b,\tau_b). \tag{23}$$

Here ∂_u and ∂_v refer to the partial derivatives with respect to the first and second arguments in $\widetilde{H}(u, v)$ respectively. Again, $\hat{\phi}_{\tau\tau}(n_b, \tau_b)$ can be found explicitly using the inflow boundary condition (19) and the parametric equations of Γ. The equation (23) is then easily solved to obtain $\hat{\phi}_{n\tau}(n_b, \tau_b)$. Next the PDE (1) under the local coordinate system is differentiated with respect to n, and evaluated at (n_b, τ_b) to obtain

$$\partial_u \widetilde{H}(\hat{\phi}_n(n_b,\tau_b), \hat{\phi}_\tau(n_b,\tau_b))\hat{\phi}_{nn}(n_b,\tau_b) + \partial_v \widetilde{H}(\hat{\phi}_n(n_b,\tau_b), \hat{\phi}_\tau(n_b,\tau_b))\hat{\phi}_{n\tau}(n_b,\tau_b) = \hat{f}_n(n_b,\tau_b). \tag{24}$$

As $\hat{\phi}_{n\tau}(n_b, \tau_b)$ has already been obtained, the only unknown is the second order normal derivative $\hat{\phi}_{nn}(n_b, \tau_b)$ which we can solve for readily. Similarly, we can follow this procedure to find the values of $\hat{\phi}_{nnn}(n_b, \tau_b)$ and $\hat{\phi}_{nnnn}(n_b, \tau_b)$ in order to obtain the fifth order approximation in the equation (20). Again, the fifth order approximation in (20) is used for the local solver with the MR-WENO5 scheme. For the local solver with the MR-WENO3 scheme, we take the first three terms at the right hand side of (20) to obtain the third order approximation of $\phi(x_a, y_a)$. As indicated in [6, 31], the inverse Lax-Wendroff procedure is suitable for the case that the inflow boundary is not a single point.

2.2.3 Factored Eikonal approach

When the inflow boundary Γ is a singular source-point (i.e. the corresponding solution of Eikonal equation has singularity at the source-point), we can *not* use either the Richardson extrapolation procedure because the solution is singular at Γ, or the inverse Lax-Wendroff procedure since the inflow boundary is a single point. In this case, factored Eikonal approach developed in [4, 14, 16] is an efficient boundary treatment method. Here we briefly describe the method. More details can be found in [4, 14, 16].

For the Eikonal equation (2), $|\nabla\phi| = f$, if it has a singular source-point at (x_0, y_0), the multiplicative factorization is to decompose the solution $\phi(x, y)$ by $\phi(x, y) = \phi_0(x, y)u(x, y)$, and correspondingly the right-hand-side function $f(x, y)$ by $f(x, y) = f_0(x, y)\alpha(x, y)$. The idea is that the factor $\phi_0(x, y)$ captures the source singularity such that the underlying function $u(x, y)$ is smooth in a neighborhood of the source point. $\phi_0(x, y)$ satisfies the equation

$$|\nabla\phi_0| = f_0. \tag{25}$$

f_0 is often chosen as some constant, so $\phi_0(x, y)$ is the travel-time corresponding to the constant velocity field $1/f_0$ and it can be written out explicitly. For example, if we take $f_0 = 1$, then $\phi_0(x, y) = \sqrt{(x - x_0)^2 + (y - y_0)^2}$, which is the distance function to the source point. The function ϕ_0 contains the source singularity. Since it is factored out from ϕ, the remaining function $u(x, y)$ is smooth in a neighborhood of the source. $u(x, y)$ satisfies the multiplicative factored Eikonal equation

$$\sqrt{\phi_0^2(u_x^2 + u_y^2) + 2\phi_0 u(\phi_{0x}u_x + \phi_{0y}u_y) + u^2 f_0^2} = f. \tag{26}$$

We use the Lax-Friedrichs numerical Hamiltonian with the multi-resolution WENO approximations to the derivatives as the local solver to solve the multiplicative factored Eikonal equation (26) for $u(x, y)$.

Alternatively, the Eikonal equation (2) can be factored additively by the decomposition $\phi(x, y) = \phi_0(x, y) + u(x, y)$ and $f(x, y) = f_0(x, y) + \alpha(x, y)$, as in [16]. $f_0(x, y)$ and $\phi_0(x, y)$ are chosen and written out explicitly in the same way as that in the multiplicative factored Eikonal approach. $u(x, y)$ satisfies the following additive factored Eikonal equation

$$\sqrt{(u_x^2 + u_y^2) + 2(\phi_{0x}u_x + \phi_{0y}u_y) + f_0^2} = f. \tag{27}$$

Similarly, the Lax-Friedrichs numerical Hamiltonian with the multi-resolution WENO approximations to the derivatives as the local solver is used to solve the additive factored Eikonal equation (27) for $u(x, y)$.

Finally, the solution to the original Eikonal equation (2) is recovered by either $\phi(x, y) = \phi_0(x, y)u(x, y)$ or $\phi(x, y) = \phi_0(x, y) + u(x, y)$.

2.3 Algorithm summary: multi-resolution WENO fast sweeping methods

We summarize the high order multi-resolution WENO fast sweeping methods as following:

1. *Initialization*: for the problems that the Richardson extrapolation procedure or the inverse Lax-Wendroff procedure is used for inflow boundary, according to the given boundary condition $\phi(x, y) = g(x, y)$, $(x, y) \in \Gamma$, follow the methods described in Sec. 2.2 to obtain numerical values at grid points whose distances to Γ are less than or equal to $2h$ for the MR-WENO3 local solver or $3h$ for the MR-WENO5 local solver. If a grid point is on Γ, exact value from the condition $\phi(x, y) = g(x, y)$ is directly used to specify the numerical value at that point. The numerical values at these grid points near inflow boundary are fixed during the iteration. For the problems that the factored Eikonal approach is used, the initial values for $u(x, y)$ at these grid points near inflow boundary (i.e., the singular source-point) are assigned to be 1 in solving the multiplicative factored Eikonal equation (26) and to be 0 in solving the additive factored Eikonal equation (27). Different from the previous two approaches (i.e., the Richardson extrapolation and the inverse Lax-Wendroff), the numerical values at these grid points near inflow boundary are not fixed and will be updated along with values at all other grid points, following the suggestion and analysis in [16]. At all other grid points, if the Godunov numerical Hamiltonian is used, the initial guesses are set as the solution from the first order Godunov fast sweeping method [36]; if the Lax-Friedrichs numerical Hamiltonian is utilized, in general big values are used as the initial guesses, unless otherwise indicated.

2. *Iterations*: if the Godunov numerical Hamiltonian is used for discretization, update $\phi_{i,j}^{new}$ as in (3) and (4); if the Lax-Friedrichs numerical Hamiltonian is used for discretization, update $\phi_{i,j}^{new}$ as in (6). Gauss-Seidel iterations with four alter-

nating direction sweepings are used for the updates:

$$\begin{aligned}
&(1) \quad i = 1 : N, \quad j = 1 : M;\\
&(2) \quad i = N : 1, \quad j = 1 : M;\\
&(3) \quad i = N : 1, \quad j = M : 1;\\
&(4) \quad i = 1 : N, \quad j = M : 1.
\end{aligned}$$

Here one sweeping is counted as one iteration. Multi-resolution WENO approximations described in Section 2.1 are computed for the derivative terms in (4) and (6), using the newest available numerical values in the multi-resolution WENO schemes' stencils according to the philosophy of Gauss-Seidel iterations. For both of the local solvers using either the Godunov numerical Hamiltonian or the Lax-Friedrichs numerical Hamiltonian, high order extrapolations are applied for the ghost points when calculating the third order or the fifth order MR-WENO approximations of derivatives for grid points near or on the outflow boundary of the computational domain. In this paper, a third order extrapolation is used.

3. *Convergence*: the iterations stop and the convergence is declared whenever the iteration residue

$$||\phi^{new} - \phi^{old}||_{L_1} \leq \delta,$$

where $||\cdot||_{L_1}$ denotes the L_1 norm and δ is a specified threshold value.

In simulations of this paper, the convergence threshold value is taken as $\delta = 10^{-12}$, unless otherwise specified.

3 Numerical Experiments

In this section, We apply the proposed high order multi-resolution WENO fast sweeping methods to some typical benchmark problems. Both of the local solvers with the MR-WENO3 scheme and the MR-WENO5 scheme are tested to verify the accuracy, nonlinear stability to resolve non-smooth solutions, and algorithm efficiency. Examples are shown to demonstrate the absolute convergence of the new fifth order fast sweeping method and its advantage by comparing with the earlier method in [31]. Following the approach in [31], a third order extrapolation is applied on the outflow boundary, which maintains efficient convergence of the fast sweeping iterations and does not affect the desired fifth order accuracy away from the outflow boundary for the MR-WENO5 scheme. This is verified by measuring the numerical errors in the inner region of the computational domain, which is slightly away from the outflow boundary. Note that in this section, the notation "N" in all numerical tables denotes the number of computational cells in each of the spatial directions of the domain.

Example 1 We solve the Eikonal equation (2) with

$$f(x, y) = \frac{\pi}{2}\sqrt{\sin^2(\pi + \frac{\pi}{2}x) + \sin^2(\pi + \frac{\pi}{2}y)}, \tag{28}$$

and the inflow boundary Γ is the origin point $(0,0)$. The computational domain is $[-1,1]^2$. The exact solution is a smooth function

$$\phi(x,y) = \cos(\pi + \frac{\pi}{2}x) + \cos(\pi + \frac{\pi}{2}y). \tag{29}$$

The Richardson extrapolation procedure is used to treat the inflow boundary, namely to approximate numerical values at the grid points in the boxes of $[-2h, 2h]^2$ for the MR-WENO3 local solver and $[-3h, 3h]^2$ for the MR-WENO5 local solver. For the outflow boundary, which is the boundary of the box $[-1,1]^2$, we use a third order extrapolation. The numerical error is measured in an inner box $[-0.9, 0.9]^2$ of the computational domain, in order to avoid the influence of the outflow boundary. To be consistent, errors for both of local solvers with the MR-WENO3 scheme and the MR-WENO5 scheme are computed in this way even though the third order extrapolation does not affect the accuracy of the MR-WENO3 scheme near the outflow boundary. Since we are using the Godunov numerical Hamiltonian for this problem, the solution from the first order Godunov fast sweeping method [36] is used as the initial guess for all the other grid points outside of the neighborhood of the inflow boundary, as described in the section 2.3. The L_1 errors, L_∞ errors, their numerical accuracy orders, number of iterations for the fast sweeping schemes to converge, and total CPU time costs are reported in Table 1 for both of the MR-WENO3 fast sweeping scheme and the MR-WENO5 fast sweeping scheme. It is observed that the desired 3rd order and 5th order accuracy are obtained for both of fast sweeping schemes respectively. From the number of iterations for the fast sweeping schemes to converge and the total CPU time costs on successively refined meshes, the computational complexity of these fast sweeping schemes is approximately slightly larger than linear, but much less than quadratic. This is consistent with our observations for the earlier WENO fast sweeping methods in [35, 31].

Example 2 We solve the Eikonal equation (2) with $f(x,y) = 1$ and Γ is a circle of center $(0,0)$ with radius 0.5. The computational domain is $[-1,1]^2$. The exact solution is the distance function to the circle Γ, and has a singularity at the center of the circle where the characteristics converge. In the simulation, the Godunov numerical Hamiltonian and the inverse Lax-Wendroff procedure for the inflow boundary are used. Similar to the previous example, numerical errors are measured 0.15 away from the singularity of the solution and inside the box of $[-0.9, 0.9]^2$, to avoid the influence of singularity and outflow numerical boundary. Also the numerical errors are measured in the same domain for both the MR-WENO3 fast sweeping method and the MR-WENO5 fast sweeping method to be consistent. The L_1 errors, L_∞ errors, their numerical accuracy orders, number of iterations for the fast sweeping schemes to converge, and total CPU time costs are reported in Table 2 for both of the MR-WENO3 fast sweeping scheme and the MR-WENO5 fast sweeping scheme. It is observed that the desired 3rd order and 5th order accuracy are obtained in smooth region of the solution for both of fast sweeping schemes respectively. As the previous example, the number of iterations for the fast sweeping schemes to converge and the total CPU time costs reported in Table 2 show that on refined meshes, the computational complexity of the multi-resolution WENO fast sweeping schemes is approximately slightly larger than linear, but much less than quadratic.

MR-WENO3 fast sweeping						
N	L_1 error	L_1 order	L_∞ error	L_∞ order	Iteration number	CPU(s)
80	6.54142e-06		1.12740e-05		104	0.779004
160	7.08282e-07	3.207	1.23094e-06	3.195	140	3.28049
320	8.60817e-08	3.041	1.49619e-07	3.040	200	13.9968
640	1.07507e-08	3.001	1.86532e-08	3.004	328	66.8125
MR-WENO5 fast sweeping						
N	L_1 error	L_1 order	L_∞ error	L_∞ order	Iteration number	CPU(s)
80	1.39497e-07		3.26720e-07		156	0.959227
160	4.75239e-09	4.875	7.35226e-09	5.474	204	4.14169
320	1.53120e-10	4.956	2.28830e-10	5.006	272	18.3607
640	4.85519e-12	4.979	7.24154e-12	4.982	416	94.3821

Table 1: Example 1. Γ is a single point and the solution is smooth. L_1 errors, L_∞ errors, numerical accuracy orders, number of iterations for the schemes to converge, and total CPU time costs.

MR-WENO3 fast sweeping						
N	L_1 error	L_1 order	L_∞ error	L_∞ order	Iteration number	CPU(s)
80	2.58729e-06		6.13068e-05		260	0.211494
160	3.73390e-07	2.793	9.79816e-06	2.645	108	0.35854
320	4.89945e-08	2.930	1.28070e-06	2.936	148	1.92983
640	6.27109e-09	2.966	1.61609e-07	2.986	224	11.5815
MR-WENO5 fast sweeping						
N	L_1 error	L_1 order	L_∞ error	L_∞ order	Iteration number	CPU(s)
80	1.03172e-06		2.92456e-05		120	0.187746
160	2.96781e-08	5.120	1.53767e-06	4.249	156	0.967422
320	7.94527e-10	5.223	2.46292e-09	9.286	204	5.01093
640	2.43188e-11	5.030	7.87152e-11	4.968	292	29.0089

Table 2: Example 2. Γ is a circle, and the errors are measured in the smooth region 0.15 away from the singularity. L_1 errors, L_∞ errors, numerical accuracy orders, number of iterations for the schemes to converge, and total CPU time costs.

Example 3 We solve the Eikonal equation (2) with $f(x,y) = 1$, and Γ consists of two circles of radius 0.5 with centers at $(-1,0)$ and $(\sqrt{1.5},\ 0)$ respectively. The computational domain is $[-3,3]^2$. The exact solution is the distance function to the circles Γ, which has singularities at the center of each circle and the line that is of equal distance to the two circles. In the simulation, the Godunov numerical Hamiltonian and the inverse Lax-Wendroff procedure for the inflow boundary are used. The L_1 errors, L_∞ errors, their numerical accuracy orders, number of iterations for the fast sweeping schemes to converge, and total CPU time costs are reported in Table 3, with numerical errors measured 0.15 away from the singularities and inside the box of $[-2.7, 2.7]^2$ (away from the outflow boundary). We observe that the desired 3rd order and 5th order accuracy are obtained in smooth region of the solution for both methods. From the number of iterations for the fast sweeping schemes to converge and the total CPU time costs reported in Table 3, we observe that except an outlier case of simulation on the 161×161 mesh by the MR-WENO5 fast sweeping method, the computational complexity of the multi-resolution WENO fast sweeping schemes is approximately slightly larger than linear, but much less than quadratic. Numerical solutions on the 161×161 mesh are presented in Fig. 4 for the MR-WENO3 and the MR-WENO5 fast sweeping methods. It is observed that the singularities of the solution are resolved stably for both methods. In Fig. 5, we show the comparison of the iteration residue history on the 161×161 mesh for the fifth order fast sweeping schemes based on the multi-resolution WENO (MR-WENO5) local solver developed in this paper and the classical WENO (WENO5) local solver in [31]. The iteration residue of the classical WENO5 fast sweeping scheme hangs at the 10^{-8} level, while the iteration residue of the MR-WENO5 fast sweeping scheme can converge to round-off error level. The absolute convergence of the new MR-WENO5 fast sweeping scheme, which is an advantage over the classical WENO5 fast sweeping scheme in [31], is verified here.

Example 4 The Eikonal equation (2) with $f(x,y) = 1$ is solved, and Γ is a sector of three quarters of a circle centered at $(0,0)$ and the radius 0.5, closed with the x-axis and y-axis in the first quadrant. It can be described as

$$\begin{aligned}\Gamma = \ & \{(x,y) : \sqrt{x^2+y^2} = 0.5, \text{if } x \le 0 \text{ or } y \le 0\} \cup \{(x,0) : 0 \le x \le 0.5\} \\ & \cup \{(0,y) : 0 \le y \le 0.5\}.\end{aligned}$$

The computational domain is $[-2,2]^2$. The exact solution is the distance function to Γ. Singularities at the corners of the sector Γ give rise to different scenarios in different regions, which include both shocks and rarefaction waves. For the inflow boundary treatment of this problem, the inverse Lax-Wendroff procedure can be used for most part of Γ, except the point $(0,0)$. The point $(0,0)$ is a singular source-point and here we present two different approaches to deal with it. The first approach is to follow [35, 31] and assign exact values of the solution for the grid points in a small neighborhood of $(0,0)$ in the third quadrant. These assigned exact values are fixed during the iterations. As discussed in [35], this is one way to avoid the accuracy loss due to singular source-point, for a high order fast sweeping method. However this approach could be difficult to be used for complex problems when the exact solution near the singular source-point is hard to find. The second approach is to use the factored Eikonal approach

MR-WENO3 fast sweeping						
N	L_1 error	L_1 order	L_∞ error	L_∞ order	Iteration number	CPU(s)
80	5.83354e-05		8.31336e-04		132	0.114744
160	6.62235e-06	3.139	2.62113e-04	1.665	168	0.563717
320	9.83594e-07	2.751	3.23836e-05	3.017	164	2.21535
640	1.35682e-07	2.858	4.25734e-06	2.927	252	13.2930
MR-WENO5 fast sweeping						
N	L_1 error	L_1 order	L_∞ error	L_∞ order	Iteration number	CPU(s)
80	1.32275e-04		5.74845e-04		136	0.239394
160	5.55693e-06	4.573	4.14713e-05	3.793	704	4.34305
320	1.56725e-07	5.148	8.49752e-07	5.609	228	5.83857
640	5.23955e-09	4.903	1.93666e-08	5.455	324	32.6200

Table 3: Example 3. Γ consists of two circles, and the errors are measured in the smooth region 0.15 away from the singularities. L_1 errors, L_∞ errors, numerical accuracy orders, number of iterations for the schemes to converge, and total CPU time costs.

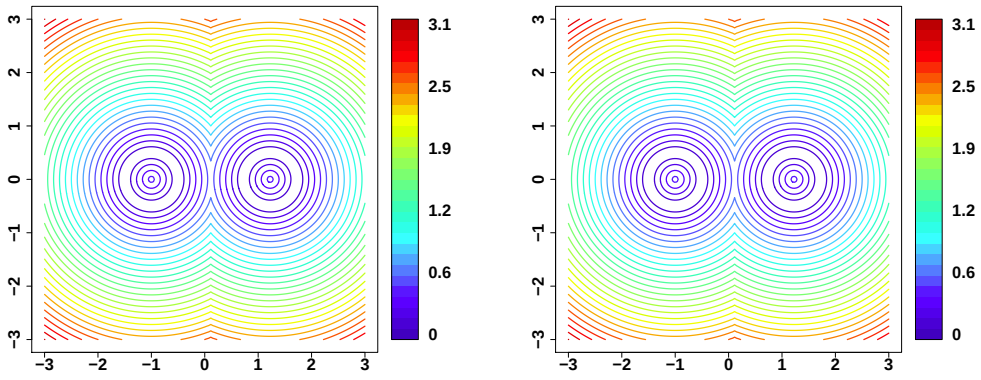

Figure 4: Example 3, Γ consists of two circles. Numerical solutions on the 161×161 mesh, 30 equally spaced contour lines. Left: the MR-WENO3 fast sweeping scheme; right: the MR-WENO5 fast sweeping scheme.

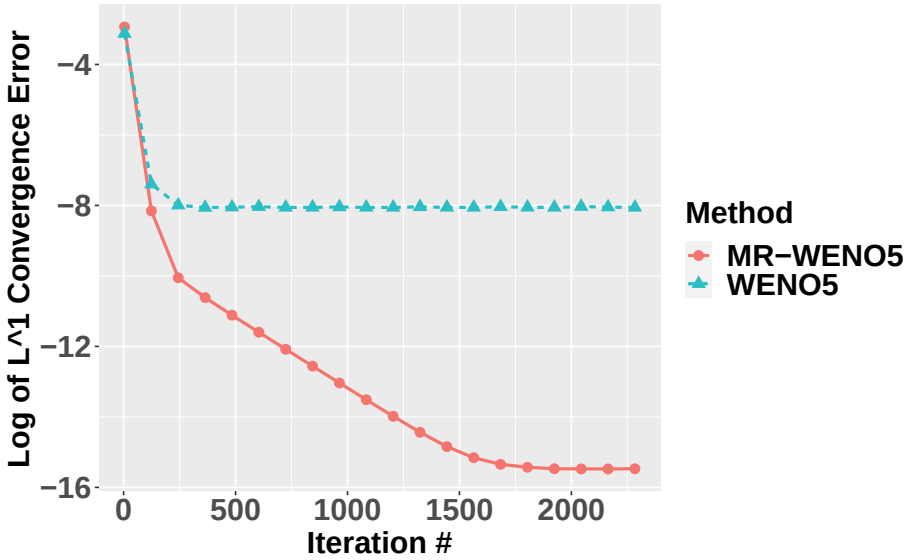

Figure 5: Example 3, Γ consists of two circles. Comparison of the iteration residue history on the 161×161 mesh for the fifth order fast sweeping schemes based on the multi-resolution WENO (MR-WENO5) local solver and the classical WENO (WENO5) local solver.

discussed in the section 2.2.3 to treat the singular source-point $(0,0)$, which does not need assignments of exact values of the solution. Here we present the results of both approaches. Similar to [31], the numerical errors are computed in the smooth region outside the circle $\sqrt{x^2+y^2}=0.5$, with $x<0$ or $y<0$, and inside the box $[-1.8,1.8]^2$.

First, we apply the first approach and solve the Eikonal equation (2) directly. For the initialization step, exact values of the solution are assigned for the grid points in the third quadrant, whose distances to the singular source-point $(0,0)$ are less than or equal to $2h$ and $3h$ for the MR-WENO3 fast sweeping method and the MR-WENO5 fast sweeping method respectively, with the inverse Lax-Wendroff procedure applied to the rest of the inflow boundary Γ. The Godunov numerical Hamiltonian is used in the simulation. The L_1 errors, L_∞ errors, their numerical accuracy orders, number of iterations for the fast sweeping schemes to converge, and total CPU time costs are reported in Table 4, with numerical errors measured in the smooth region. As previous examples, we observe that the desired 3rd order and 5th order accuracy are obtained in that smooth region of the solution for both methods. Note that correct accuracy orders and algorithm convergence can be achieved without changing the value of ϵ in the WENO weights on different meshes for the proposed multi-resolution WENO fast sweeping schemes, while ϵ has to be adjusted on different meshes for the classical WENO fast sweeping methods in [31]. This demonstrates an advantage of the new WENO fast sweeping methods. Also, the number of iterations for the fast sweeping schemes to converge and the total CPU time costs indicate that the computational complexity of the proposed multi-resolution WENO fast sweeping schemes is approximately

slightly larger than linear, but much less than quadratic. As a further illustration of the efficiency of high order fast sweeping method, we compare the MR-WENO5 fast sweeping method with the time marching approach based on the Godunov numerical Hamiltonian to solve the steady-state problem, as in [35]. For the time marching approach, the MR-WENO5 spatial discretization and a third order TVD Runge-Kutta scheme [26] in time direction are used, with the CFL number taken to be 0.6 as in [35]. The other setups such as the initial guesses, boundary treatments, the convergence threshold value are the same as those in the MR-WENO5 fast sweeping method. The numerical errors, accuracy orders, number of iterations and CPU time costs using the time marching approach are also shown in Table 4. Here we count each time-stepping of the third order Runge-Kutta scheme, which includes three stages, as three iterations. Results in Table 4 show that both L_1 and L_∞ errors of the time marching approach are almost the same as those of the MR-WENO5 fast sweeping method, up to round-off errors. However, comparisons of the number of iterations and CPU time costs show that the MR-WENO5 fast sweeping method is much more efficient than the time marching approach on refined meshes. For example, on the 161×161 mesh, the MR-WENO5 fast sweeping method is almost 4 times faster than the time marching approach in terms of CPU time cost, and it only needs less than 1/3 of the iteration steps to converge to the steady-state solution. On more refined meshes, we see more savings of the computational time with the MR-WENO5 fast sweeping method. On the 641×641 mesh, the MR-WENO5 fast sweeping method is more than 6 times faster than the time marching approach, and it needs about 1/6 of the iteration steps to converge. Contour plots of the numerical solutions on the 321×321 mesh and three dimensional pictures of the numerical solutions on the 161×161 mesh are presented in Fig. 6 and Fig. 7 respectively for the MR-WENO3 and the MR-WENO5 fast sweeping methods. It is observed that the singularities of the solution are resolved stably for both methods. Similar to Example 3, the absolute convergence of the new MR-WENO5 fast sweeping scheme, which is an advantage over the classical WENO5 fast sweeping scheme in [31], is verified in this example as well. In Fig. 8, we show the comparison of the iteration residue history on the 161×161 mesh for the MR-WENO5 fast sweeping method and the classical WENO5 fast sweeping method in [31]. The iteration residue of the classical WENO5 fast sweeping scheme hangs at the $10^{-8} \sim 10^{-9}$ level, while the iteration residue of the MR-WENO5 fast sweeping scheme can converge to round-off error level.

Now we solve the problem by the second approach, namely, using the factored Eikonal approach to treat the singular source-point $(0, 0)$, which does not need assignments of exact values of the solution and is more effective in real applications. The additive factored Eikonal approach is applied and the factored Eikonal equation (27) is solved for $u(x, y)$ by the multi-resolution WENO fast sweeping methods with the Lax-Friedrichs numerical Hamiltonian. We choose $f_0 = 1$, so $\phi_0 = \sqrt{x^2 + y^2}$ which captures the singularity of the singular source-point $(0, 0)$. Different from the first approach to assign values of the exact solution, based on the suggestion and analysis in [16], we initialize $u(x, y)$ with the value 0.0 for grid points in the third quadrant, whose distances to the singular source-point $(0, 0)$ are less than or equal to $2h$ and $3h$ for the MR-WENO3 fast sweeping method and the MR-WENO5 fast sweeping method respectively. The numerical values at these grid points are not fixed and will be updated along with values at all other grid points except that the value at the inflow source-point

MR-WENO3 fast sweeping						
N	L_1 error	L_1 order	L_∞ error	L_∞ order	Iteration number	CPU(s)
80	1.89771e-05		9.42907e-05		260	0.220134
160	3.30197e-06	2.523	6.31940e-06	3.899	132	0.474460
320	4.79186e-07	2.785	9.04267e-07	2.805	188	2.55406
640	6.37289e-08	2.911	1.20988e-07	2.902	300	15.9044
MR-WENO5 fast sweeping						
N	L_1 error	L_1 order	L_∞ error	L_∞ order	Iteration number	CPU(s)
80	1.48005e-04		5.99484e-04		276	0.431125
160	1.88660e-06	6.294	1.19014e-05	5.655	192	1.21731
320	6.56049e-08	4.846	3.83969e-07	4.954	260	6.47989
640	2.47151e-09	4.730	7.96686e-09	5.591	388	38.4895
MR-WENO5 time marching						
N	L_1 error	L_1 order	L_∞ error	L_∞ order	Iteration number	CPU(s)
80	1.48005e-04		5.99484e-04		336	0.577057
160	1.88660e-06	6.294	1.19014e-05	5.655	618	4.25032
320	6.56049e-08	4.846	3.83969e-07	4.954	1173	31.9010
640	2.47150e-09	4.730	7.96629e-09	5.591	2262	252.536

Table 4: Example 4. Γ is a sector of three quarters of a circle, and the errors are measured in a smooth region. L_1 errors, L_∞ errors, numerical accuracy orders, number of iterations for the schemes to converge, and total CPU time costs for the MR-WENO3 fast sweeping scheme, the MR-WENO5 fast sweeping scheme, and the MR-WENO5 time marching scheme. The Eikonal equation (2) is solved directly, with values of the exact solution assigned for grid points near the singular source-point $(0, 0)$ in the third quadrant.

$(0, 0)$ is fixed as $u(0, 0) = 0$. For all other grid points near the inflow boundary Γ, the inverse Lax-Wendroff procedure is applied as that described in the section 2.2.2. Table 5 shows the L_1 errors, L_∞ errors, their numerical accuracy orders, number of iterations for the schemes to converge, and total CPU time costs for the MR-WENO3 fast sweeping method and the MR-WENO5 fast sweeping method respectively, to solve the Eikonal equation (2) using the factored Eikonal approach. The desired 3rd order and 5th order accuracy are obtained in that smooth region of the solution for both methods. Note that more iterations are needed for the fast sweeping methods to converge in the second approach than the first approach since the Lax-Friedrichs numerical Hamiltonian is used to solve the factored Eikonal equation whereas the Godunov numerical Hamiltonian is used in the first approach. In general fast sweeping methods based on the Lax-Friedrichs numerical Hamiltonian need more iterations to converge than fast sweeping methods based on the Godunov numerical Hamiltonian, as discussed in [35]. However the factored Eikonal approach is more practically effective since there is no need to find exact solution of the PDE in the neighborhood of a singular source-point, which could be difficult for a complex problem in applications.

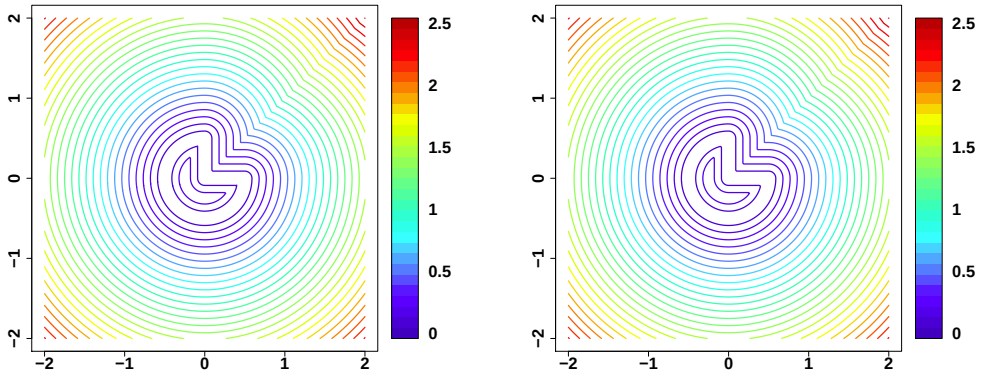

Figure 6: Example 4, Γ is a sector of three quarters of a circle. Numerical solutions on the 321×321 mesh, 30 equally spaced contour lines. The Eikonal equation (2) is solved directly, with values of the exact solution assigned for grid points near the singular source-point $(0, 0)$ in the third quadrant. Left: the MR-WENO3 fast sweeping scheme; right: the MR-WENO5 fast sweeping scheme.

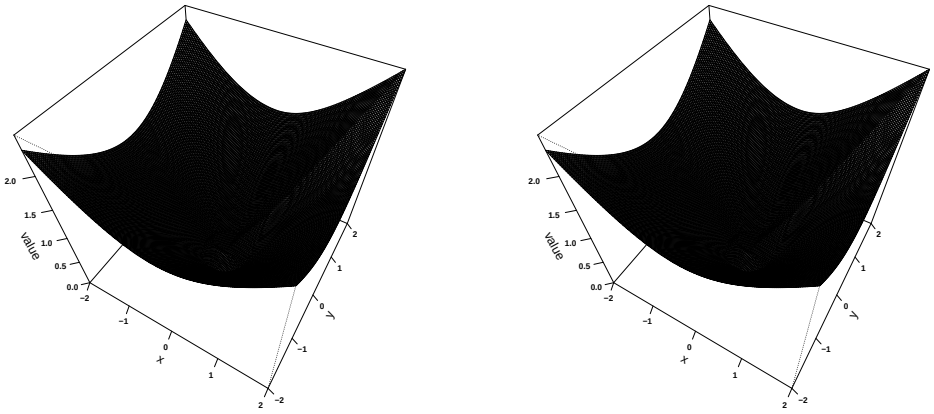

Figure 7: Example 4, Γ is a sector of three quarters of a circle. Numerical solutions on the 161×161 mesh, three dimensional plots. The Eikonal equation (2) is solved directly, with values of the exact solution assigned for grid points near the singular source-point $(0, 0)$ in the third quadrant. Left: the MR-WENO3 fast sweeping scheme; right: the MR-WENO5 fast sweeping scheme.

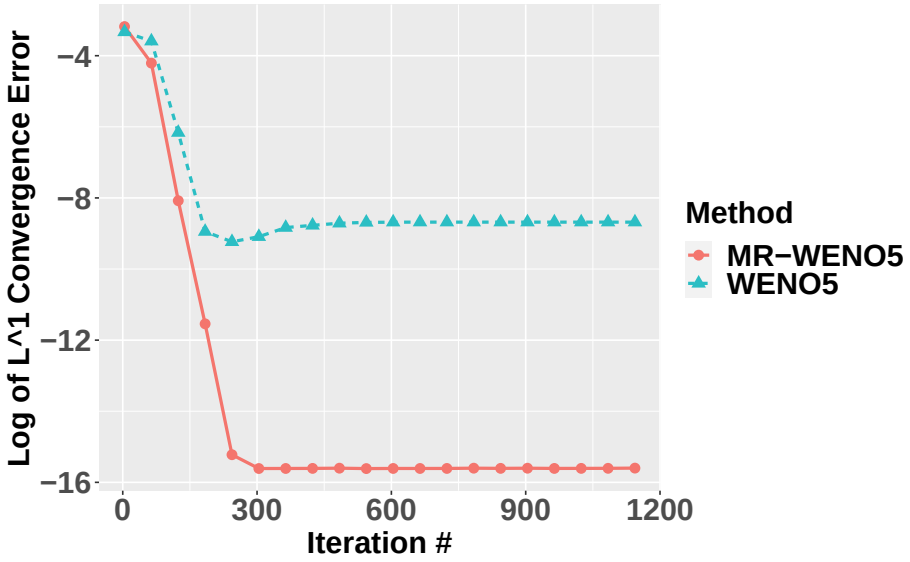

Figure 8: Example 4, Γ is a sector of three quarters of a circle. Comparison of the iteration residue history on the 161×161 mesh for the fifth order fast sweeping schemes based on the multi-resolution WENO (MR-WENO5) local solver and the classical WENO (WENO5) local solver.

MR-WENO3 fast sweeping						
N	L_1 error	L_1 order	L_∞ error	L_∞ order	Iteration number	CPU(s)
80	6.10408e-04		8.11404e-04		288	0.2703
160	1.16026e-04	2.395	2.52579e-04	1.684	440	1.6396
320	1.27975e-05	3.181	2.63137e-05	3.263	736	10.5743
640	1.26354e-06	3.340	1.97496e-06	3.736	1324	76.6524
MR-WENO5 fast sweeping						
N	L_1 error	L_1 order	L_∞ error	L_∞ order	Iteration number	CPU(s)
80	2.04002e-04		5.85643e-04		316	0.886523
160	2.34388e-06	6.444	1.02468e-05	5.837	476	5.13529
320	8.49839e-08	4.786	2.01773e-07	5.666	808	33.4467
640	3.32533e-09	4.676	5.77887e-09	5.126	1480	242.74

Table 5: Example 4. Γ is a sector of three quarters of a circle, and the errors are measured in a smooth region. L_1 errors, L_∞ errors, numerical accuracy orders, number of iterations for the schemes to converge, and total CPU time costs for the MR-WENO3 fast sweeping scheme and the MR-WENO5 fast sweeping scheme. The Eikonal equation (2) is solved by using the factored Eikonal approach to treat the singular source-point $(0, 0)$.

Example 5 (Shape-from-shading I) We solve a shape-from-shading problem modeled by the Eikonal equation (2) with

$$f(x,y) = 2\pi\sqrt{[\cos(2\pi x)\sin(2\pi y)]^2 + [\cos(2\pi y)\sin(2\pi x)]^2}. \tag{30}$$

The computational domain Ω is $[0,1]^2$. The inflow boundary

$$\Gamma = \{(\frac{1}{4},\frac{1}{4}),(\frac{3}{4},\frac{3}{4}),(\frac{3}{4},\frac{1}{4}),(\frac{1}{4},\frac{3}{4}),(\frac{1}{2},\frac{1}{2})\} \cup \partial\Omega,$$

which consists of a set of five isolated points and the boundary of the domain Ω. $\phi(x,y) = 0$ is prescribed at the boundary of the unit square $[0,1]^2$. Solution of shape-from-shading problem is a shape function under vertical lighting [22]. We consider the following two cases:

Case 1. $g(\frac{1}{4},\frac{1}{4}) = g(\frac{3}{4},\frac{3}{4}) = 1$, $g(\frac{1}{4},\frac{3}{4}) = g(\frac{3}{4},\frac{1}{4}) = -1$, and $g(\frac{1}{2},\frac{1}{2}) = 0$. The exact solution of this case is a smooth function $\phi(x,y) = \sin(2\pi x)\sin(2\pi y)$.

Case 2. $g(\frac{1}{4},\frac{1}{4}) = g(\frac{3}{4},\frac{3}{4}) = g(\frac{1}{4},\frac{3}{4}) = g(\frac{3}{4},\frac{1}{4}) = 1$, and $g(\frac{1}{2},\frac{1}{2}) = 2$. The exact solution of this case is

$$\phi(x,y) = \begin{cases} \max(|\sin(2\pi x)\sin(2\pi y)|, 1+\cos(2\pi x)\cos(2\pi y)), \\ \quad \text{if } |x+y-1| < \frac{1}{2} \text{ and } |x-y| < \frac{1}{2}; \\ |\sin(2\pi x)\sin(2\pi y)|, \quad \text{otherwise}, \end{cases} \tag{31}$$

which is not smooth.

The inverse Lax-Wendroff procedure is applied to the grid points near the inflow boundary $\partial\Omega$. However, for the isolated points in Γ, the inverse Lax-Wendroff procedure cannot be applied. Our numerical simulations also find that in this example, the Richardson extrapolation procedure and the factored Eikonal approach do not yield desirable results (e.g. desired accuracy orders or correct convergence) if we apply them to the isolated points in Γ. This is also observed in [31] in which the Richardson extrapolation procedure is used. The reason could be due to the fact that at these isolated points, the right hand side function $f = 0$ and they correspond to multiple places with ∞ wave-velocity, which gives certain singularity in the PDE. Further investigation is needed to study this. Here, as in [31, 35], values of the exact solution are assigned to the grid points around these isolated points. In this problem, the exact solution is set to the grid points whose distances to the isolated points are less than or equal to $3h_0$ where $h_0 = 1/80$ is the mesh size of the coarsest mesh in the mesh refinement study, i.e., in a small box with a length of $6h_0$ around the isolated points, for simulations by using either the 3rd order schemes or the 5th order schemes on all meshes. In this example, the convergence threshold value is taken as $\delta = 10^{-14}$ to ensure that it is smaller than the numerical errors of the 5th order schemes on refined meshes, and for the purpose of consistency, this iteration-stopping criterion $\delta = 10^{-14}$ is applied to all simulations here. The L_1 errors, L_∞ errors, their numerical accuracy orders, number of iterations for the MR-WENO fast sweeping schemes to converge, and total CPU time costs are reported in Table 6, with numerical errors measured on the whole computational domain. The desired 3rd order and 5th order accuracy of the corresponding MR-WENO3 and MR-WENO5 fast sweeping schemes are obtained for Case 1 which has a smooth solution. For Case 2, since its solution is not smooth,

reduced orders of accuracy are observed as expected. Again, the number of iterations and the total CPU time costs in Table 6 indicate that the computational complexity of the developed MR-WENO fast sweeping schemes is approximately slightly larger than linear, but much less than quadratic. Contour plots of the numerical solutions on the 161×161 mesh are presented in Fig. 9 for the MR-WENO5 fast sweeping method, which shows high resolution of the scheme.

For a further study, we solve this example using the classical WENO3 and WENO5 fast sweeping methods [35, 31] with the same iteration-stopping criterion and boundary treatments as the MR-WENO fast sweeping methods, then compare their numerical results. The L_1 errors, L_∞ errors, their numerical accuracy orders, number of iterations for the classical WENO fast sweeping schemes to converge, and total CPU time costs are reported in Table 7, with numerical errors also measured on the whole computational domain. The desired accuracy orders of the classical WENO fast sweeping schemes are obtained. For Case 1 which has a smooth solution, the classical WENO fast sweeping methods have smaller numerical errors than the MR-WENO fast sweeping methods, while their numerical errors are comparable for Case 2 whose solution is not smooth. It is observed that in this example, the computational costs (CPU times) for the classical WENO fast sweeping methods to converge are fewer than those for the MR-WENO fast sweeping methods. The comparison here shows that although the MR-WENO fast sweeping methods are often more robust than the classical WENO fast sweeping methods as verified in previous examples, the classical WENO fast sweeping methods could be more efficient for some problems.

Similar to Example 4, we compare the MR-WENO5 fast sweeping method with the time marching approach, i.e., the third order TVD Runge-Kutta scheme [26] in time direction, to solve the steady-state problem. The setup of the time marching approach is the same as that in Example 4. The iteration-stopping criterion is $\delta = 10^{-14}$ as well. The numerical results are reported in Table 8 for both cases of this example, which show that both L_1 and L_∞ errors of the time marching approach are almost the same as those of the MR-WENO5 fast sweeping method, up to round-off errors. However, similar to what is observed in Example 4, comparisons of the number of iterations and CPU time costs show that the MR-WENO5 fast sweeping method is much more efficient than the time marching approach. For example, on the 81×81 mesh for Case 1, the MR-WENO5 fast sweeping method is more than 3 times faster than the time marching approach in terms of CPU time, and it only needs less than 1/3 of the iteration steps to converge. On more refined meshes, the efficiency advantage of the MR-WENO5 fast sweeping method is more significant. On the 641×641 mesh, the MR-WENO5 fast sweeping method is more than 6 times faster and only requires around 1/6 of the iteration steps to converge, compared with the time marching approach. Similar performance is also observed for Case 2.

Example 6 (Shape-from-shading II) We solve shape-from-shading problems with different right-hand-side functions: the Eikonal equation (2) with

$$\text{Case } 1 : f(x, y) = \sqrt{(1 - |x|)^2 + (1 - |y|)^2}; \tag{32}$$

$$\text{Case } 2 : f(x, y) = 2\sqrt{y^2(1 - x^2)^2 + x^2(1 - y^2)^2}. \tag{33}$$

Case 1, smooth solution, MR-WENO3 fast sweeping						
N	L_1 error	L_1 order	L_∞ error	L_∞ order	Iteration number	CPU(s)
80	3.08683e-05		1.38099e-04		96	0.059921
160	2.43149e-06	3.666	1.09679e-05	3.654	128	0.311129
320	2.62701e-07	3.210	1.19099e-06	3.203	176	1.61581
640	3.17336e-08	3.049	1.43670e-07	3.051	280	10.0124
Case 1, smooth solution, MR-WENO5 fast sweeping						
N	L_1 error	L_1 order	L_∞ error	L_∞ order	Iteration number	CPU(s)
80	1.53399e-06		7.08566e-06		148	0.184093
160	4.69073e-08	5.031	2.14102e-07	5.049	180	0.870113
320	1.42293e-09	5.043	6.40063e-09	5.064	244	4.60098
640	4.37295e-11	5.024	1.94897e-10	5.037	360	26.6364
Case 2, non-smooth solution, MR-WENO3 fast sweeping						
N	L_1 error	L_1 order	L_∞ error	L_∞ order	Iteration number	CPU(s)
80	1.27019e-04		1.74023e-03		88	0.056234
160	2.68242e-05	2.243	6.93377e-04	1.328	108	0.261471
320	5.13732e-06	2.384	2.45814e-04	1.496	156	1.46265
640	8.60095e-07	2.578	8.69836e-05	1.499	244	8.71795
Case 2, non-smooth solution, MR-WENO5 fast sweeping						
N	L_1 error	L_1 order	L_∞ error	L_∞ order	Iteration number	CPU(s)
80	4.66054e-05		8.07956e-04		132	0.181125
160	8.03202e-06	2.537	2.71909e-04	1.571	160	0.780074
320	1.20487e-06	2.737	9.00918e-05	1.594	216	4.09713
640	1.99342e-07	2.596	2.93939e-05	1.616	316	23.4165

Table 6: Example 5. Shape-from-shading I. The errors are measured on the whole computational domain. L_1 errors, L_∞ errors, numerical accuracy orders, number of iterations for the schemes to converge, and total CPU time costs for the MR-WENO3 fast sweeping scheme and the MR-WENO5 fast sweeping scheme.

Case 1, smooth solution, classical WENO3 fast sweeping						
N	L_1 error	L_1 order	L_∞ error	L_∞ order	Iteration number	CPU(s)
80	1.59523e-05		7.23288e-05		116	0.039857
160	1.96880e-06	3.018	8.99880e-06	3.001	148	0.201625
320	2.48588e-07	2.985	1.13211e-06	2.991	208	1.10409
640	3.12993e-08	2.990	1.41881e-07	2.996	316	6.64534
Case 1, smooth solution, classical WENO5 fast sweeping						
N	L_1 error	L_1 order	L_∞ error	L_∞ order	Iteration number	CPU(s)
80	4.32432e-08		2.07602e-07		148	0.112989
160	6.69969e-10	6.012	3.28094e-09	5.984	184	0.452352
320	1.93346e-11	5.115	9.50508e-11	5.109	244	2.32526
640	6.04574e-13	4.999	2.96557e-12	5.002	360	13.3898
Case 2, non-smooth solution, classical WENO3 fast sweeping						
N	L_1 error	L_1 order	L_∞ error	L_∞ order	Iteration number	CPU(s)
80	1.24434e-04		1.73415e-03		104	0.037573
160	2.67226e-05	2.219	6.93186e-04	1.323	128	0.16807
320	5.13381e-06	2.380	2.45806e-04	1.496	184	0.975041
640	8.59980e-07	2.578	8.69833e-05	1.499	276	5.78431
Case 2, non-smooth solution, classical WENO5 fast sweeping						
N	L_1 error	L_1 order	L_∞ error	L_∞ order	Iteration number	CPU(s)
80	4.84508e-05		8.42811e-04		136	0.102246
160	8.04384e-06	2.591	2.72651e-04	1.628	160	0.395243
320	1.20484e-06	2.739	9.00953e-05	1.598	216	2.03614
640	1.99331e-07	2.596	2.93935e-05	1.616	316	12.0428

Table 7: Example 5. Shape-from-shading I. The errors are measured on the whole computational domain. L_1 errors, L_∞ errors, numerical accuracy orders, number of iterations for the schemes to converge, and total CPU time costs for the classical WENO3 fast sweeping scheme and the classical WENO5 fast sweeping scheme.

Case 1, smooth solution, MR-WENO5 with TVD-RK3						
N	L_1 error	L_1 order	L_∞ error	L_∞ order	Iteration number	CPU(s)
80	1.53399e-06		7.08566e-06		528	0.671747
160	4.69073e-08	5.031	2.14102e-07	5.049	642	3.25205
320	1.42293e-09	5.043	6.40064e-09	5.064	1110	21.9713
640	4.37317e-11	5.024	1.94907e-10	5.037	2058	164.952
Case 2, non-smooth solution, MR-WENO5 with TVD-RK3						
N	L_1 error	L_1 order	L_∞ error	L_∞ order	Iteration number	CPU(s)
80	4.66054e-05		8.07956e-04		429	0.552009
160	8.03202e-06	2.537	2.71909e-04	1.571	531	2.67272
320	1.20487e-06	2.737	9.00918e-05	1.594	948	18.7246
640	1.99342e-07	2.596	2.93939e-05	1.616	1779	142.823

Table 8: Example 5. Shape-from-shading I. The errors are measured on the whole computational domain. L_1 errors, L_∞ errors, numerical accuracy orders, number of iterations for the schemes to converge, and total CPU time costs for the MR-WENO5 time marching scheme.

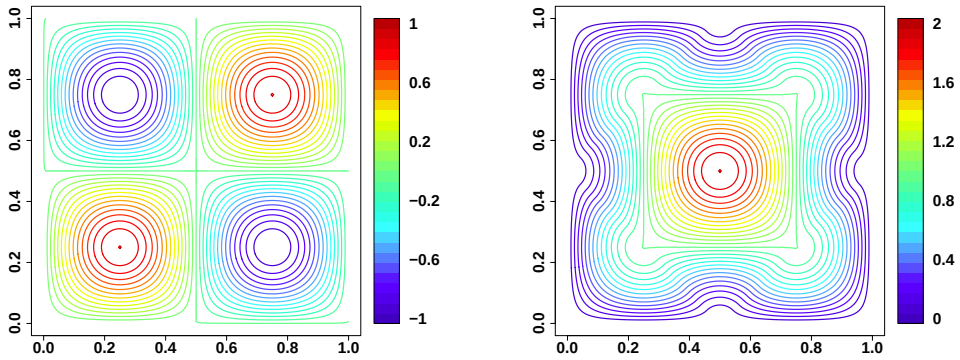

Figure 9: Example 5. Shape-from-shading I. Numerical solutions of the MR-WENO5 fast sweeping method on the 161×161 mesh, 30 equally spaced contour lines. Left: Case 1; right: Case 2.

The computational domain is $[-1,1]^2$. Here the inflow boundary Γ is the whole boundary of the square domain. The boundary condition $\phi(x,y)=0$ is prescribed on Γ. An additional boundary condition $\phi(0,0)=1$ is also prescribed for Case 2. The exact solutions for these two cases are

$$\text{Case } 1: \phi(x,y) = (1-|x|)(1-|y|); \tag{34}$$

$$\text{Case } 2: \phi(x,y) = (1-x^2)(1-y^2). \tag{35}$$

In the simulations, the inverse Lax-Wendroff procedure is used for the inflow boundary treatment. For the extra source-point $(0,0)$ in Case 2, similar to Example 5, values of the exact solution need to be assigned to the grid points around it. Here exact values are assigned to the grid points whose distances to the source-point $(0,0)$ are less than or equal to $2h$ and $3h$ for the MR-WENO3 fast sweeping method and the MR-WENO5 fast sweeping method respectively. The Godunov numerical Hamiltonian is used in this example. The L_1 errors, L_∞ errors, number of iterations for the fast sweeping schemes to converge, and total CPU time costs are reported in Table 9, with numerical errors measured in the whole domain. Note that the exact solution of Case 1 is a piecewise bi-linear polynomial and the exact solution of Case 2 is a bi-quadratic polynomial, so the numerical solutions by the third order and the fifth order fast sweeping schemes are accurate up to round-off errors with refined meshes. The exact solution of Case 1 is simpler than that of Case 2, which makes the fast sweeping iterations of Case 1 (only four iterations) converge much faster than those of Case 2, and the numerical errors for Case 1 be smaller than those of Case 2. Convergence behavior of the fast sweeping iterations for Case 2 is similar to previous examples, i.e., the computational complexity of the MR-WENO fast sweeping schemes is approximately slightly larger than linear, but much less than quadratic. For the problem of Case 1, it is also interesting to find that in [31], ϵ needs to be adjusted to a very small value 10^{-14} for obtaining numerical errors at the round-off level when numerical errors are measured in the whole domain. However, here for the MR-WENO fast sweeping methods, we are able to obtain similar results without any adjustment of parameters in the local solvers. This shows improvements on the robustness of the new MR-WENO fast sweeping methods over the previous methods in [31].

Example 7 We use an example with smooth solution from [4, 14] to test the accuracy of the developed MR-WENO fast sweeping methods for solving factored Eikonal equation. Consider the Eikonal equation (2) with

$$f = \sqrt{f_0^2 + 2.0[g_x(x-x_0) + g_y(y-y_0)]}, \tag{36}$$

where f_0 is chosen to be 2.0, $(g_x, g_y) = (0,-3)$, and $(x_0, y_0) = (0.25, 0)$ is the location of the source-point. The computational domain is $[0, 0.5] \times [-0.25, 0.25]$. In this case, the exact solution ϕ is smooth and known to be

$$\phi = \overline{f}^2\sigma - (g_x^2 + g_y^2)\frac{\sigma^3}{6}, \tag{37}$$

where

$$\overline{f} = \sqrt{f_0^2 + g_x(x-x_0) + g_y(y-y_0)} \tag{38}$$

Case 1, MR-WENO3 fast sweeping				
N	L_1 error	L_∞ error	Iteration number	CPU(s)
80	4.50844e-17	4.44089e-16	4	0.006206
160	4.29558e-17	4.44089e-16	4	0.024738
320	6.85490e-17	1.11022e-15	4	0.086768
640	1.00931e-16	1.22125e-15	4	0.331557
Case 1, MR-WENO5 fast sweeping				
N	L_1 error	L_∞ error	Iteration number	CPU(s)
80	3.65696e-17	4.44089e-16	4	0.013005
160	4.08243e-17	5.55112e-16	4	0.048206
320	6.77552e-17	1.11022e-15	4	0.174695
640	9.67345e-17	1.22125e-15	4	0.687068
Case 2, MR-WENO3 fast sweeping				
N	L_1 error	L_∞ error	Iteration number	CPU(s)
80	2.21797e-09	1.34712e-08	68	0.057293
160	7.68787e-11	4.46730e-10	88	0.294458
320	2.66785e-12	1.10892e-10	132	1.74832
640	3.53976e-13	3.43715e-10	228	12.1515
Case 2, MR-WENO5 fast sweeping				
N	L_1 error	L_∞ error	Iteration number	CPU(s)
80	2.04941e-11	1.39635e-10	100	0.143326
160	8.88327e-13	2.07816e-11	120	0.734434
320	2.52924e-13	7.32117e-11	168	4.09827
640	2.13078e-13	2.45299e-10	284	27.5583

Table 9: Example 6. Shape-from-shading II. The errors are measured on the whole computational domain. L_1 errors, L_∞ errors, number of iterations for the schemes to converge, and total CPU time costs for the MR-WENO3 fast sweeping scheme and the MR-WENO5 fast sweeping scheme.

and

$$\sigma = \frac{\sqrt{2\left(\overline{f}^2 - \sqrt{\overline{f}^4 - (g_x^2 + g_y^2)\left((x-x_0)^2 + (y-y_0)^2\right)}\right)}}{\sqrt{g_x^2 + g_y^2}}. \tag{39}$$

Here we apply the multiplicative factored Eikonal approach and numerically solve the multiplicative factored Eikonal equation (26) for $u(x, y)$ using the MR-WENO fast sweeping methods with the Lax-Friedrichs numerical Hamiltonian, and finally recover the solution to the original Eikonal equation (2) by $\phi(x, y) = \phi_0(x, y)u(x, y)$. By choosing $f_0 = 2.0$, the travel-time corresponding to the constant velocity field $1/f_0$ is $\phi_0 = 2\sqrt{(x-0.25)^2 + y^2}$. As in Example 4, we do not need to assign exact values of the solution to grid points around the source-point, hence it is an effective approach to treat a single source-point inflow boundary condition in real applications since it could be still difficult to find exact solution near the source-point. Based on the suggestion and analysis in [16], we initialize $u(x, y)$ with the value 1.0 for grid points whose distances to the source-point $(0.25, 0)$ are less than or equal to $2h$ and $3h$ for the MR-WENO3 fast sweeping method and the MR-WENO5 fast sweeping method respectively. The numerical values at these grid points are not fixed and will be updated along with values at all other grid points except that the value at the source-point $(0.25, 0)$ is fixed as $u(0.25, 0) = 1.0$. Table 10 shows the L_1 errors, L_∞ errors, their numerical accuracy orders, number of iterations for the schemes to converge, and total CPU time costs for the MR-WENO3 fast sweeping method and the MR-WENO5 fast sweeping method respectively, to solve the Eikonal equation (2) using the multiplicative factored Eikonal approach. The numerical errors are measured in the region $[0.05, 0.45] \times [-0.2, 0.2]$, which is slightly away from the outflow boundary to avoid its influence as in previous examples. The desired accuracy orders are obtained for both fast sweeping methods. Here the iteration-stopping criterion is taken to be $\delta = 10^{-14}$, so that the iteration residue of the MR-WENO5 fast sweeping method is smaller than the numerical errors of the scheme on refined meshes. The total CPU time costs indicate that the computational complexity of the MR-WENO fast sweeping schemes for solving the factored Eikonal equation is larger than linear, but still much less than quadratic, which is consistent with the other examples. Contour plots of the numerical solutions on the 161×161 mesh are shown in Fig. 10 for both schemes.

Example 8 (Sinusoidal model) We use an example from [14] to test the ability of the developed MR-WENO fast sweeping methods with the factored Eikonal approach to resolve singular source-point and non-smooth solution. Consider the Eikonal equation (2) with $f = 1/v$, where the velocity field v is given by

$$v(x, y) = 1 + 0.2 \sin(0.5\pi y) \sin(3\pi(x + 0.55)). \tag{40}$$

The computational domain is $[-1, 1] \times [0, 2]$ and the singular source-point is located at $(0, 0)$. The multiplicative factored Eikonal approach is used to deal with the singular source-point. For this example, we choose $f_0 = 1$, and the travel-time corresponding to this constant velocity field $1/f_0$ is $\phi_0 = \sqrt{x^2 + y^2}$ which captures the singularity of the source-point. Similar to Example 7, we initialize $u(x, y)$ in the multiplicative

MR-WENO3 fast sweeping						
N	L_1 error	L_1 order	L_∞ error	L_∞ order	Iteration number	CPU(s)
20	5.38950e-06		8.49364e-05		220	0.017771
40	1.68396e-07	5.000	5.72833e-06	3.890	440	0.106363
80	1.80136e-09	6.547	2.36721e-08	7.919	900	0.776252
160	2.08869e-10	3.108	6.27122e-10	5.238	1820	6.04344
MR-WENO5 fast sweeping						
N	L_1 error	L_1 order	L_∞ error	L_∞ order	Iteration number	CPU(s)
20	1.66081e-08		1.79065e-07		252	0.032243
40	3.29611e-10	5.655	5.55895e-09	5.010	520	0.217915
80	1.91853e-12	7.425	5.11886e-11	6.763	1080	1.69737
160	5.23406e-14	5.196	2.11164e-13	7.921	2216	13.8093

Table 10: Example 7. L_1 errors, L_∞ errors, numerical accuracy orders, number of iterations for the schemes to converge, and total CPU time costs for the MR-WENO3 fast sweeping scheme and the MR-WENO5 fast sweeping scheme. The Eikonal equation (2) is solved by using the multiplicative factored Eikonal approach to treat the source-point $(0.25, 0)$.

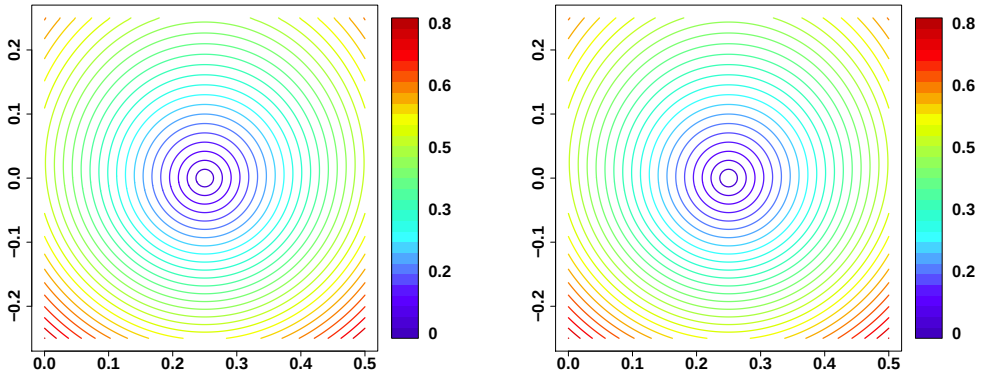

Figure 10: Example 7. Numerical solutions on the 161×161 mesh, 30 equally spaced contour lines. The Eikonal equation (2) is solved by using the multiplicative factored Eikonal approach to treat the source-point $(0.25, 0)$. Left: the MR-WENO3 fast sweeping scheme; right: the MR-WENO5 fast sweeping scheme.

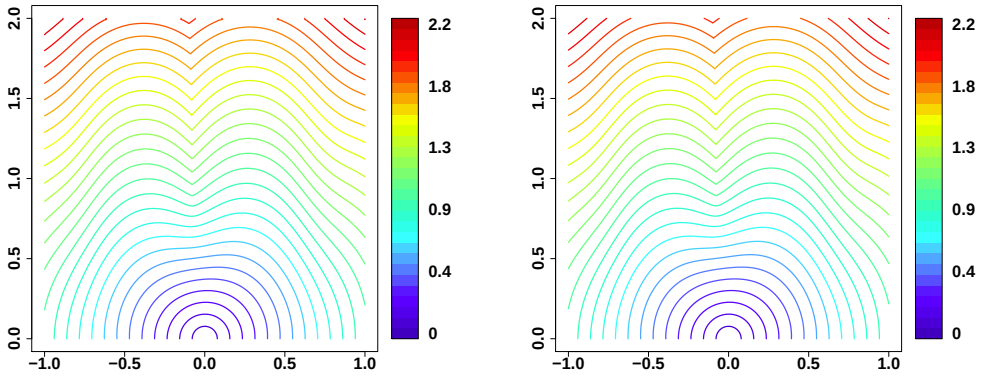

Figure 11: Example 8, Sinusoidal model. Numerical solutions on the 321×321 mesh, 30 equally spaced contour lines. The Eikonal equation (2) is solved by using the multiplicative factored Eikonal approach to treat the singular source-point $(0, 0)$. Left: the MR-WENO3 fast sweeping scheme; right: the MR-WENO5 fast sweeping scheme.

factored Eikonal equation (26) with the value 1.0 for grid points whose distances to the source-point $(0, 0)$ are less than or equal to $2h$ and $3h$ for the MR-WENO3 fast sweeping method and the MR-WENO5 fast sweeping method respectively. The numerical values at these grid points are not fixed and will be updated along with values at all other grid points except that the value at the source-point $(0, 0)$ is fixed as $u(0, 0) = 1.0$. The multiplicative factored Eikonal equation (26) for $u(x, y)$ is solved using the MR-WENO fast sweeping methods with the Lax-Friedrichs numerical Hamiltonian, and the solution to the original Eikonal equation (2) is finally recovered by $\phi(x, y) = \phi_0(x, y)u(x, y)$. The numerical solutions of the MR-WENO3 fast sweeping method and the MR-WENO5 fast sweeping method on the 321×321 mesh are reported in Fig. 11, which shows that the singularities in the non-smooth solution are resolved well and stably.

Example 9 (Marmousi model) We solve the Marmousi model in [28]. In [4, 14], a first order and a third order fast sweeping methods were used to simulate this model. The Marmousi velocity model is often used in the study of seismic data. It is the Eikonal equation (2) with the right hand side $f = 1/v$ where the velocity field v is obtained from an open source data set, i.e., the Marmousi data set [28], and it demonstrates significant velocity changes. Here the data set has the size 80×80. The velocity data and their locations in the domain are rescaled by a factor of 10^{-4}, so that the computational domain is ranging from $x = 0.4$ to $x = 0.7$ and $y = 0.0$ to $y = 0.3$. The singular source-point is located at $(0.6, 0.26)$. The Marmousi velocity field is shown in Fig. 12.

The MR-WENO5 fast sweeping method with the multiplicative factored eikonal approach is applied for dealing with the singular source-point and computing the model's corresponding travel-time solution ϕ. ϕ_0 is chosen to be the distance function to the

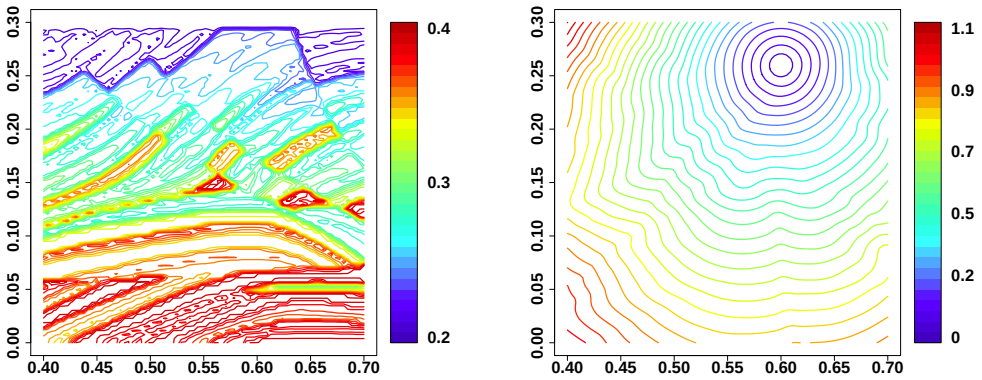

Figure 12: Example 9, Marmousi model. Left: contour plot of the Marmousi velocity field, 30 equally spaced contour lines; right: numerical solution of the traveltime by the MR-WENO5 fast sweeping method on the 80×80 mesh, 30 equally spaced contour lines. The Eikonal equation (2) is solved by using the multiplicative factored Eikonal approach to treat the singular source-point $(0.6, 0.26)$.

singular source-point $(0.6, 0.26)$ for capturing the singularity of the source-point. Initialization of $u(x, y)$ in the multiplicative factored Eikonal equation (26) is similar to the previous examples, i.e., we assign the value 1.0 for the grid points whose distances to the source-point $(0.6, 0.26)$ are less than or equal to $3h$. The numerical values at these grid points are updated along with values at all other grid points by the iterations of the scheme. The multiplicative factored Eikonal equation (26) for $u(x, y)$ is solved using the MR-WENO5 fast sweeping method with the Lax-Friedrichs numerical Hamiltonian, and the solution to the original Eikonal equation (2) is finally recovered by $\phi(x, y) = \phi_0(x, y)u(x, y)$. The numerical solution of the MR-WENO5 fast sweeping method on the 80×80 mesh is reported in Fig. 12, which is consistent with the results in the literature, e.g. [14].

Example 10 (Anisotropic problems) The previous examples are isotropic Eikonal equation (2). In this example, we apply the developed MR-WENO5 fast sweeping method with factored Eikonal approach to anisotropic problems with a singular source-point, specifically a problem from [15] and its variant case. Consider the anisotropic Eikonal equation with a source-point boundary condition in the following form:

$$\begin{cases} \sqrt{a(x,y)\phi_x^2 - 2c(x,y)\phi_x\phi_y + b(x,y)\phi_y^2} = 1, & (x,y) \in \Omega \setminus \{(x_0,y_0)\}, \\ \phi(x_0,y_0) = 0, \end{cases} \tag{41}$$

where $a(x, y), b(x, y), c(x, y)$ are coefficients and the source-point is located at (x_0, y_0). Here we use the additive factored Eikonal approach to deal with the singular source-

point. Namely, with the additive factorization $\phi = \phi_0 + u$ substituted into the equation (41), the factored anisotropic Eikonal equation is obtained:

$$\Big\{a(x,y)u_x^2 - 2c(x,y)u_xu_y + b(x,y)u_y^2 + 2u_x\big(a(x,y)\phi_{0x} - c(x,y)\phi_{0y}\big) \\ + 2u_y\big(b(x,y)\phi_{0y} - c(x,y)\phi_{0x}\big) + a(x,y)\phi_{0x}^2 - 2c(x,y)\phi_{0x}\phi_{0y} + b(x,y)\phi_{0y}^2\Big\}^{1/2} = 1, \tag{42}$$

where $\phi_0(x,y)$ is the viscosity solution of the simple anisotropic Eikonal equation with constant coefficients

$$\begin{cases}\sqrt{a_0{\phi_0}_x^2 - 2c_0{\phi_0}_x{\phi_0}_y + b_0{\phi_0}_y^2} = 1, & (x,y) \in \Omega \setminus \{(x_0,y_0)\},\\ \phi_0(x_0,y_0) = 0,\end{cases} \tag{43}$$

and a_0, b_0, and c_0 are the values of $a(x,y), b(x,y)$, and $c(x,y)$ at the source-point (x_0,y_0). The exact solution of the equation (43) can be found analytically as

$$\phi_0(x,y) = \sqrt{\frac{b_0(x-x_0)^2 + 2c_0(x-x_0)(y-y_0) + a_0(y-y_0)^2}{a_0b_0 - c_0^2}}, \tag{44}$$

which captures the singularity of the source-point.

We solve two specific problems. The first one is a problem in [15] where the computational domain is $[0,1]^2$ and the source-point is located at $(0.5, 0.5)$. The variable coefficients in the equation (41) are taken to be

$$a(x,y) = \frac{1.0}{e^{-2\sqrt{2(x-x_0)^2+2(x-x_0)(y-y_0)+(y-y_0)^2}}},$$
$$b(x,y) = \frac{2.0}{e^{-2\sqrt{2(x-x_0)^2+2(x-x_0)(y-y_0)+(y-y_0)^2}}},$$
$$c(x,y) = \frac{1.0}{e^{-2\sqrt{2(x-x_0)^2+2(x-x_0)(y-y_0)+(y-y_0)^2}}}.$$

Thus, by (44), $\phi_0(x,y) = \sqrt{2(x-x_0)^2 + 2(x-x_0)(y-y_0) + (y-y_0)^2}$. The exact solution of this problem is $\phi(x,y) = 1 - e^{-\sqrt{2(x-x_0)^2+2(x-x_0)(y-y_0)+(y-y_0)^2}}$. This problem is called "Case 1" here. The second problem is to modify Case 1 for a different wave propagation direction, and is named as "Case 2". The computational domain and the source-point are the same as Case 1. The variable coefficients $a(x,y), b(x,y), c(x,y)$ in the equation (41) are set to be

$$a(x,y) = \frac{2.0}{e^{-2\sqrt{4(x-x_0)^2-2(x-x_0)(y-y_0)+2(y-y_0)^2}}},$$
$$b(x,y) = \frac{4.0}{e^{-2\sqrt{4(x-x_0)^2-2(x-x_0)(y-y_0)+2(y-y_0)^2}}},$$
$$c(x,y) = \frac{-1.0}{e^{-2\sqrt{4(x-x_0)^2-2(x-x_0)(y-y_0)+2(y-y_0)^2}}}.$$

Hence $\phi_0(x,y) = \sqrt{4(x-x_0)^2 - 2(x-x_0)(y-y_0) + 2(y-y_0)^2}$. The exact solution of this problem is $\phi(x,y) = 1 - e^{-\sqrt{4(x-x_0)^2-2(x-x_0)(y-y_0)+2(y-y_0)^2}}$.

We apply the additive factored Eikonal approach and numerically solve the factored anisotropic Eikonal equation (42) for $u(x,y)$ using the MR-WENO5 fast sweeping method with the Lax-Friedrichs numerical Hamiltonian, and finally recover the solution to the original anisotropic Eikonal equation (41) by $\phi(x,y) = \phi_0(x,y) + u(x,y)$. As in previous examples of the isotropic Eikonal equations, we do not need to assign exact values of the solution to grid points around the singular source-point to achieve high order accuracy. Instead, the value at the source-point $(0.5, 0.5)$ is fixed as $u(0.5, 0.5) = 0$. For all other grid points except the source-point $(0.5, 0.5)$, we first perform 10 iterations by the first order fast sweeping method in [8] and use the obtained values as the initial guesses on them for the MR-WENO5 fast sweeping method to continue updating till the MR-WENO5 fast sweeping iterations converge. Different from the isotropic Eikonal equations, the value of ϵ in the MR-WENO5 local solver is taken as $\epsilon = 10^{-8}$ for solving the anisotropic problems here, since it is found in the numerical experiments that a smaller ϵ value leads to a better convergence behavior of the scheme. Table 11 shows the L_1 errors, L_∞ errors, their numerical accuracy orders, number of iterations for the scheme to converge, and total CPU time costs for the MR-WENO5 fast sweeping method to solve both Case 1 and Case 2 problems using the additive factored Eikonal approach. The numerical errors are measured in the region $[0.05, 0.95]^2$ which is slightly away from the outflow boundary to avoid its influence as in previous examples. The desired fifth order accuracy is obtained for both cases, which have a singular source-point. The total CPU time costs again verify that the computational complexity of the MR-WENO5 fast sweeping scheme for solving the factored anisotropic Eikonal equation is larger than linear, but still much less than quadratic, which is consistent with the previous examples for the isotropic Eikonal equations. Contour plots of the numerical solutions on the 321×321 mesh are shown in Fig. 13 for both Case 1 and Case 2.

4 Concluding Remarks

In this paper, high order accuracy multi-resolution WENO fast sweeping methods for solving static H-J equations, specifically the Eikonal equations, are developed. The new WENO fast sweeping methods for static H-J equations improve the convergence behavior of previous WENO fast sweeping methods. The fast sweeping iterations can achieve the absolute convergence, i.e., iteration residues of a higher order (e.g., the fifth order) WENO fast sweeping method can settle down to round-off errors. Inflow boundary conditions are taken care of carefully. For problems with a singular source-point inflow boundary, the effective factored Eikonal approach is applied to treat the inflow boundary, and the resulted factored Eikonal equations are solved by the new high order MR-WENO fast sweeping methods. Extensive numerical experiments, including solving isotropic and anisotropic Eikonal equations, and the corresponding factored Eikonal equations for problems with singular source-point, are performed to show the high order accuracy, stable ability to resolve solution singularities, and high efficiency of the presented absolutely convergent MR-WENO fast sweeping methods.

Case 1						
N	L_1 error	L_1 order	L_∞ error	L_∞ order	Iteration number	CPU(s)
80	3.64991e-04		5.50949e-04		732	1.40265
160	6.43508e-06	5.826	9.42713e-06	5.869	836	6.1383
320	2.99602e-07	4.425	4.10299e-07	4.522	1452	42.3065
640	9.46195e-09	4.985	1.29834e-08	4.982	2656	307.856
Case 2						
N	L_1 error	L_1 order	L_∞ error	L_∞ order	Iteration number	CPU(s)
80	3.07649e-06		5.28119e-06		296	0.595044
160	1.63710e-07	4.232	2.61949e-07	4.334	488	3.73127
320	5.31691e-09	4.944	7.98745e-09	5.035	840	25.1933
640	1.63500e-10	5.023	3.50576e-10	4.510	1560	183.118

Table 11: Example 10, Anisotropic problems. L_1 errors, L_∞ errors, numerical accuracy orders, number of iterations to converge, and total CPU time costs for the MR-WENO5 fast sweeping scheme. The anisotropic Eikonal equation (41) is solved by using the additive factored Eikonal approach to treat the singular source-point $(0.5, 0.5)$.

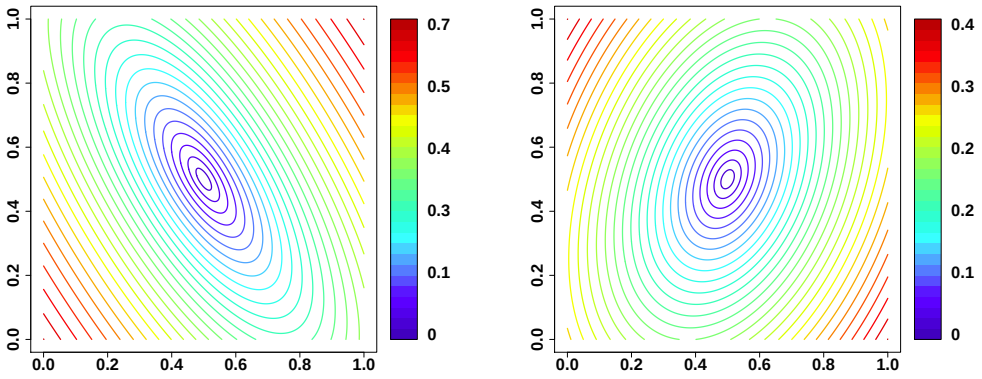

Figure 13: Example 10, Anisotropic problems. Numerical solutions of the MR-WENO5 fast sweeping scheme on the 321×321 mesh, 30 equally spaced contour lines. The anisotropic Eikonal equation (41) is solved by using the additive factored Eikonal approach to treat the singular source-point $(0.5, 0.5)$. Left: contour plot of the numerical solution of Case 1; right: contour plot of the numerical solution of Case 2.

For point-source problems whose inflow boundaries are treated by the Richardson extrapolation procedure or the factored Eikonal approach, we focus on one single source-point inflow boundary in this paper. However, the methods can be extended to treat inflow boundary with several distinct source points. This is an interesting and important topic which will be studied in details in our future work. Here we would like to outline some possible ways for such extension. If the solution is smooth around these source points, first order fast sweeping computation can be efficiently performed locally around each source point and the Richardson extrapolation procedure is applied respectively. For the cases that the characteristics from the source points intersect with each other near the source points (this may happen, e.g., if some of these source points are very close to each other), a possible approach is to sufficiently refine the mesh such that the characteristics from different source points do not intersect in a small neighborhood of these source points, then the Richardson extrapolation procedure can be applied. If the solution has singularities at these source points, i.e., they are singular source-points, a possible way to extend the current method is to first divide the whole computational domain into regions in which all grid points inside one of the regions are "closest" to one of the source points. This may be implemented by solving a Voronoi diagram problem [17] by the first order fast sweeping method, and comparing the obtained numerical solution with the factor functions $\phi_0(x, y)$ to determine the corresponding region which a grid point belongs to. Then the factored Eikonal approach is applied to every region and the corresponding factored Eikonal equation based on the singular source-point of that region will be solved by high order MR-WENO fast sweeping methods. Detailed implementation of these extensions will be carried out in the next research.

Data Availability
No data sets were generated during the current study of this paper.

Declarations

Conflict of interest
The authors declare that we have no conflict of interest.

References

[1] Borges, R., Carmona, M., Costa, B., Don, W.S.: An improved weighted essentially non-oscillatory scheme for hyperbolic conservation laws. J. Comput. Phys. 227, 3191-3211 (2008).

[2] Crandall, M.G., Lions, P.L.: Viscosity solutions of Hamilton-Jacobi equations. Trans. Amer. Math. Soc. 277, 1-42 (1983).

[3] Dijkstra, E.W.: A note on two problems in connection with graphs. Numer. Math. 1, 269-271 (1959).

[4] Fomel, S., Luo, S., Zhao, H.: Fast sweeping method for the factored eikonal equation. J. Comput. Phys. 228, 6440-6455 (2009).

[5] Huang, G., Luo, S.: Hybrid fast sweeping methods for anisotropic Eikonal equation in two-dimensional tilted transversely isotropic media. J. Sci. Comput., 84, Article 32 (2020).

[6] Huang, L., Shu, C.-W., Zhang, M.: Numerical boundary conditions for the fast sweeping high order WENO methods for solving the Eikonal equation. J. Comput. Math. 26, 1-11 (2008).

[7] Jiang, G., Shu, C.-W.: Efficient implementation of weighted ENO schemes. J. Comput. Phys. 126, 202-228, (1996).

[8] Kao, C. Y., Osher, S., Qian, J.: Lax-Friedrichs sweeping scheme for static Hamilton-Jacobi equations. J. Comput. Phys. 196, 367-391 (2004).

[9] Li, F., Shu, C.-W., Zhang, Y.-T., Zhao, H.-K.: A second order discontinuous Galerkin fast sweeping method for Eikonal equations. J. Comput. Phys. 227, 8191-8208 (2008).

[10] Li, L., Zhu, J., Shu, C.-W., Zhang, Y.-T.: A fixed-point fast sweeping WENO method with inverse Lax-Wendroff boundary treatment for steady state of hyperbolic conservation laws. Commun. Appl. Math. Comput. 5, 403-427 (2023).

[11] Li, L., Zhu, J., and Zhang, Y.-T.: Absolutely convergent fixed-point fast sweeping WENO methods for steady state of hyperbolic conservation laws. J. Comput. Phys. 443, Article 110516 (2021).

[12] Li, W., Qian, J.: Newton-type Gauss-Seidel Lax-Friedrichs high-order fast sweeping methods for solving generalized eikonal equations at large-scale discretization. Comput. Math. Appl. 79, 1222-1239 (2020).

[13] Li, Y., Cheng, J., Xia, Y., Shu, C.-W.: High order arbitrary Lagrangian-Eulerian finite difference WENO scheme for Hamilton-Jacobi equations. Commun. Comput. Phys. 26, 1530-1574 (2019).

[14] Luo, S., Qian, J.: Factored singularities and high-order Lax-Friedrichs sweeping schemes for point-source traveltimes and amplitudes. J. Comput. Phys. 230, 4742-4755 (2011).

[15] Luo, S., Qian, J.: Fast sweeping methods for factored anisotropic Eikonal equations: multiplicative and additive factors. J. Sci. Comput. 52, 360-382 (2012).

[16] Luo, S., Qian, J., Burridge R.: High-order factorization based high-order hybrid fast sweeping methods for point-source Eikonal equations. SIAM J. Numer. Anal. 52, 23-44 (2014).

[17] Miksis, Z. M., Zhang, Y.-T.: Sparse-grid implementation of fixed-point fast sweeping WENO schemes for Eikonal equations. Commun. Appl. Math. Comput. (2022). https://doi.org/10.1007/s42967-022-00209-x

[18] Osher, S., Shu, C.-W.: High-order essentially nonoscillatory schemes for Hamilton-Jacobi equations. SIAM J. Numer. Anal. 28, 907-922 (1991).

[19] Qian, J., Zhang, Y.-T., Zhao, H.-K.: Fast sweeping methods for Eikonal equations on triangular meshes. SIAM J. Numer. Anal. 45, 83-107 (2007).

[20] Qian, J., Zhang, Y.-T., Zhao, H.-K.: A fast sweeping method for static convex Hamilton-Jacobi equations. J. Sci. Comput. 31, 237-271 (2007).

[21] Ren, Y., Xiong, T., Qiu, J.: A hybrid finite difference WENO-ZQ fast sweeping method for static Hamilton-Jacobi equations. J. Sci. Comput. 83, Article 54 (2020).

[22] Rouy, E., Tourin, A.: A viscosity solutions approach to shape-from-shading. SIAM J. Numer. Anal. 29, 867-884 (1992).

[23] Sethian, J.A.: A fast marching level set method for monotonically advancing fronts. Pro. Natl. Acad. Sci. U.S.A. 93, 1591-1595 (1996).

[24] Sethian, J.A., Vladimirsky, A.: Ordered upwind methods for static Hamilton-Jacobi equations. Pro. Natl. Acad. Sci. U.S.A. 98, 11069-11074 (2001).

[25] Sethian, J.A., Vladimirsky, A.: Ordered upwind methods for static Hamilton-Jacobi equations: theory and algorithms. SIAM J. Numer. Anal. 41, 325-363 (2003).

[26] Shu, C.-W., Osher, S.: Efficient Implementation of essentially non-oscillatory shock-capturing schemes. J. Comput. Phys. 77, 439-471 (1988).

[27] Tro, S., Evans, T.M., Aslam, T.D., Lozano, E., Culp, D.B.: A second-order distributed memory parallel fast sweeping method for the Eikonal equation. J. Comput. Phys. 474, Article 111785 (2023).

[28] Versteeg, R.: The Marmousi experience: velocity model determination on a synthetic complex data set. The Leading Edge. 13, 927-936 (1994).

[29] Wu, L., Zhang, Y.-T.: A third order fast sweeping method with linear computational complexity for Eikonal equations. J. Sci. Comput. 62, 198-229 (2015).

[30] Wu, L., Zhang, Y.-T., Zhang, S., Shu, C.-W.: High order fixed-point sweeping WENO methods for steady state of hyperbolic conservation laws and its convergence study. Commun. Comput. Phys. 20, 835-869 (2016).

[31] Xiong, T., Zhang, M., Zhang, Y.-T., Shu, C.-W.: Fast sweeping fifth order WENO scheme for static Hamilton-Jacobi equations with accurate boundary treatment. J. Sci. Comput. 45, 514-536 (2010).

[32] Zhang, Y.-T., Chen, S., Li, F., Zhao, H., Shu, C.-W.: Uniformly accurate discontinuous Galerkin fast sweeping methods for Eikonal equations. SIAM J. Sci. Comput. 33, 1873-1896 (2011).

[33] Zhang, Y.-T., Shu, C.-W.: High order WENO schemes for Hamilton-Jacobi equations on triangular meshes. SIAM J. Sci. Comput. 24, 1005-1030 (2003).

[34] Zhang, Y.-T., Zhao, H.-K., Chen, S.: Fixed-point iterative sweeping methods for static Hamilton- Jacobi equations. Methods Appl. Anal. 13, 299-320 (2006).

[35] Zhang, Y.-T., Zhao, H.-K., Qian, J.: High order fast sweeping methods for static Hamilton-Jacobi equations. J. Sci. Comput. 29, 25-56 (2006).

[36] Zhao, H.-K.: A fast sweeping method for Eikonal equations. Math. Comp. 74, 603-627 (2005).

[37] Zhao, H., Osher, S., Merriman, B., Kang, M.: Implicit and non-parametric shape reconstruction from unorganized points using variational level set method. Comput. Vis. Image Underst. 80, 295-319 (2000).

[38] Zhu, J., Shu, C.-W.: Numerical study on the convergence to steady state solutions of a new class of high order WENO schemes. J. Comput. Phys. 349, 80-96 (2017).

[39] Zhu, J., Shu, C.-W.: A new type of multi-resolution WENO schemes with increasingly higher order of accuracy. J. Comput. Phys. 375, 659-683 (2018).